2022, Instituto Mexicano de Tecnología del Agua

Open Access bajo la licencia CC BY-NC-SA 4.0 (https://creativecommons.org/licenses/by-nc-sa/4.0/)

DOI: 10.24850/j-tyca-2022-02-04

Articles

Hydraulic instrumentation and its application to the Nikuradse and Prandtl-Von Kármán equations for the estimation of composite roughness in diversion tunnels Case study: Grijalva River

Instrumentación hidráulica y su aplicación a las ecuaciones de Nikuradse y Prandtl-Von Kármán para la estimación de la rugosidad compuesta en túneles de desvío. Caso de estudio: río Grijalva

Ana Alicia Palacios Fonseca[1], ORCID: https://orcid.org/0000-0001-9860-8345

Humberto Marengo Mogollón[2], ORCID: https://orcid.org/0000-0001-8829-4020

[1]Instituto Mexicano de Tecnología del agua, IMTA, Jiutepec, Morelos, Mexico, ana_palacios@tlaloc.imta.mx

[2] Engineering Faculty, Universidad Nacional Autónoma de México, Mexico City, Mexico, hmarengom@gmail.com

2022, Instituto Mexicano de Tecnología del Agua

Open Access bajo la licencia CC BY-NC-SA 4.0 (https://creativecommons.org/licenses/by-nc-sa/4.0/)

Corresponding author: Ana Alicia Palacios Fonseca, ana_palacios@tlaloc.imta.mx, anapalf27@gmail.com

Abstract

In the recent hydroelectric power plants built in Mexico (P.H. El Cajón, P.H. La Yesca, and Grijalva River tunnels), the diversion tunnels have been designed with a combination of materials: hydraulic concrete in its template and concrete cast in its walls and vault, which allows to reduce hydraulic losses and get a greater discharge capacity to guarantee the hydrological safety of the dam during the build time, in addition to achieving considerable cost savings. To monitor this capacity, several instrumentation projects have been carried out, recording the hydraulic variables in different sections, in addition to estimating the representative parameter of the composite roughness.

This article relates how estimates the composite roughness parameter in diversion tunnels, in a case study: "Communication tunnels of the Grijalva River", upstream of the Penitas Hydroelectric Power Plant, using hydraulic instrumentation to measure, among other variables, the speed in the area near to the wall. And applying the boundary layer theories of Nikuradse and Prandtl-Von Kármán to determine the equivalent roughness in the walls, as well as the review of 17 empirical equations to finally obtain the representative composite roughness of the tunnels.

Open Access bajo la licencia CC BY-NC-SA 4.0 (https://creativecommons.org/licenses/by-nc-sa/4.0/)

Keywords: Hydraulic instrumentation, composite roughness, diversion tunnels, velocity profiles, Nikuradse, Prandtl-Von Kármán, boundary layer, free-surface flow, dam safety.

Resumen

En los recientes proyectos hidroeléctricos construidos en México (P.H. El Cajón, P.H. La Yesca y túneles del río Grijalva) se han diseñado las obras de desvío con una combinación de materiales: concreto hidráulico en su plantilla y concreto lanzado en sus paredes y bóveda, lo que permite reducir las pérdidas hidráulicas y obtener una mayor capacidad de descarga para garantizar la seguridad hidrológica de la presa durante el tiempo de construcción, además de lograr considerables ahorros en los costos. Para monitorear dicha capacidad se han realizado diversos proyectos de instrumentación, lo que permite registrar las variables hidráulicas en diferentes secciones, además de estimar el parámetro representativo de la rugosidad compuesta.

Este artículo trata sobre la estimación del parámetro de rugosidad compuesta en túneles de desvío con caso de estudio: "túneles de comunicación del río Grijalva", localizados aguas arriba de la Central Hidroeléctrica Peñitas, utilizando instrumentación hidráulica que permite medir, entre otras variables, la velocidad en la zona cercana a la pared. Y aplicando las teorías de capa límite de Nikuradse y de Prandtl-Von Kármán determinar la rugosidad equivalente en las paredes, así como la revisión de 17 ecuaciones empíricas para obtener finalmente la rugosidad compuesta representativa de los túneles.

Open Access bajo la licencia CC BY-NC-SA 4.0 (https://creativecommons.org/licenses/by-nc-sa/4.0/)

Palabras clave: instrumentación hidráulica, rugosidad compuesta, túneles de desvío, perfiles de velocidad, Nikuradse, Prandtl-Von Kármán, capa límite, flujo a superficie libre, seguridad de presas.

Received: 04/03/2020

Accepted: 01/03/2021

Introduction

The Federal Electricity Commission (CFE) through the Hydropower Projects Coordination (CPH) along with the Hydraulics Laboratory have carried out several hydraulic instrumentation projects since 2008: in the Cajón dam, Yesca dam, and Grijalva River tunnels. In the Yesca dam several structures were instrumented to study their hydraulic behavior: the diversion tunnels; the generation elements, the discharge channel and oscillation chamber; the spillway; as well as the river downstream of the dam; and the reservoir. These instrumentation projects and studies consist mainly of the installation of pressure sensors or cells and Doppler gauges to calculate velocity and flow rate, as well as other variables such as the study of the composite roughness.

Open Access bajo la licencia CC BY-NC-SA 4.0 (https://creativecommons.org/licenses/by-nc-sa/4.0/)

In 2007, as a result of the 1077 mm of rainfall accumulated from October 28th to November 3rd in the Grijalva River in Chiapas, there was a landslide of 55 million cubic meters of earth and rock on the right bank that caused a blockage in the river 800 m long and 300 m wide, posing a serious safety risk for the Penitas dam which in the case of breakage could generate an unregulated flood. In addition to this, serious damage to downstream and upstream populations could be caused due to the reservoir overflow. Moreover, after the landslide, the connection between the reservoirs upstream of the fall and the Penitas dam was reduced to a channel measuring 930 m long and 70 m wide (Figure 1).

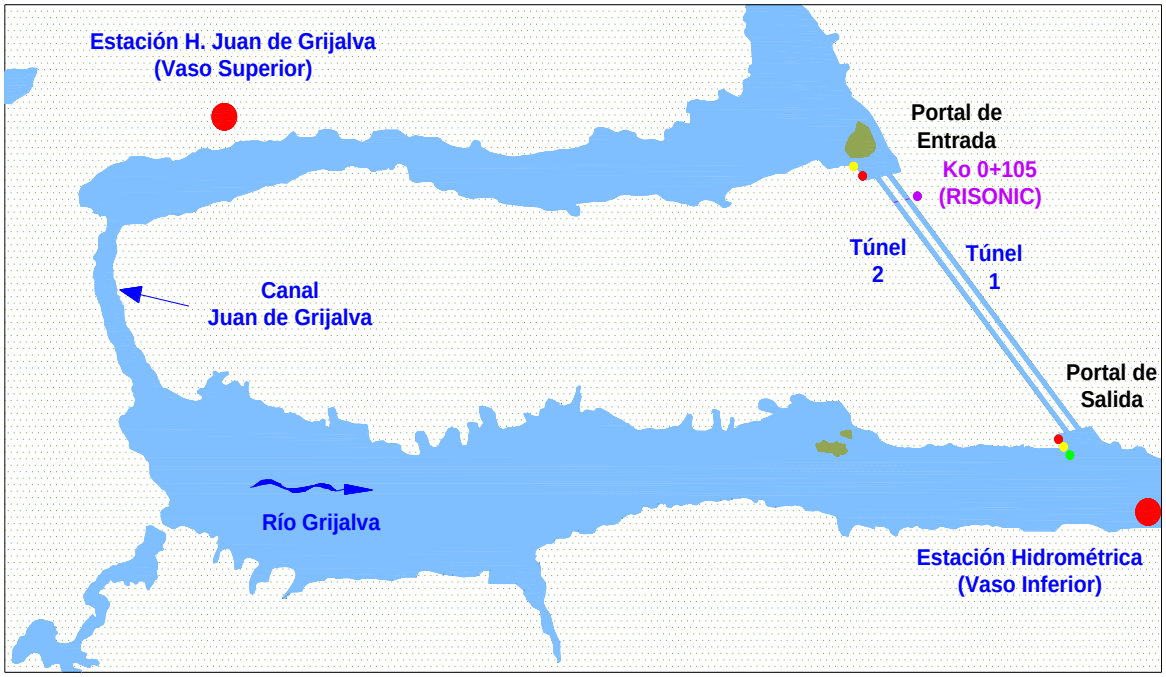

Figure 1. Location of the communication tunnels of the Grijalva River and the Juan de Grijalva channel after the landslide.

Tecnología y ciencias del agua, ISSN 2007-2422, 13(2), DOI: 10.24850/j-tyca-2022-02-04

Open Access bajo la licencia CC BY-NC-SA 4.0 (https://creativecommons.org/licenses/by-nc-sa/4.0/)

Among the actions taken to deal with flows of up to 3 500 m^3/s, were: 1. Building a channel in the reduction zone along the course of the river; 2. A temporary suspension of the generation of the Malpaso (upstream); 3. Building two 14x14 m portal section tunnels to complement the capacity of the river between the Malpaso and Penitas dams. The 3rd option for the tunnels requires monitoring for efficiency in hydraulic conduction, as well as in natural geological movements of structure, through hydraulic and geotechnical measurement instruments.

Hydraulic instrumentation was used to measure hydraulic levels, flow rates, and velocity profiles in defined sections, both in low water and rainy periods. The composite roughness parameter representative of the tunnel was also studied, which would allow for the hydraulic capacity to be defined.

The main objective of this work is to present a methodology to obtain the composite roughness parameter representative of the tunnels in the Grijalva River from direct measurements near the wall and apply the Prandtl-Von Kármán boundary layer theories and the Nikuradse equivalent roughness.

The specific objectives are 1) to study the hydraulic performance of the tunnels using hydraulic instrumentation; 2) to estimate the wall roughness parameter from velocity measurements in the boundary layer zone; 3) to estimate the composite roughness parameter through point measurements and applying Prandtl-Von Kármán and Nikuradse boundary layer theories; 4) to analyze a mathematical model and the

Tecnología y ciencias del agua, ISSN 2007-2422, 13(2), DOI: 10.24850/j-tyca-2022-02-04

Open Access bajo la licencia CC BY-NC-SA 4.0 (https://creativecommons.org/licenses/by-nc-sa/4.0/)

minimum square error (MSE) to find the best empirical equation for the composite roughness calculation, and 5) to obtain a roughness-flow curve.

This will aid in the design of hydraulic tunnels with composite roughness as well as help it in its efficiency with discharge hydraulic capacity. This research was carried out under real operating conditions.

Background

Safety of tunnels and the composite roughness

According to Marengo (2019), some considerations must be taken into account when designing and constructing tunnels. There is the experience during the construction of the Aguamilpa Hydropower Project: two extraordinary floods occurred and put the design conditions of the dam and the diversion tunnels to the test. It consisted of two 16 x 16 m portal section tunnels, a 1 100 m and 1 200 m long (Tunnel 1 and Tunnel 2, respectively), for a maximum flood of 6 700 m^3/s, in addition to a 10 m fusible tunnel and a channel on the right bank. In 1990, from August 11

Open Access bajo la licencia CC BY-NC-SA 4.0 (https://creativecommons.org/licenses/by-nc-sa/4.0/)

to 22, there was a flood of 5 300 m^3/s which caused an increase in the reservoir of 102.60 m above sea level. In 1992, from January 16 to 20, there was another flood of 10,800 m^3/s of instantaneous discharge and a maximum daily discharge of 9 334 m^3/s. This caused the reservoir level to rise from 70 m above sea level to 108 m above sea level, which provoked the upstream overflow. The tunnel fusegate had to be opened and flooding began between the cofferdam and the dam to prevent further damage and the collapse of the structure. Therefore, the maximum level of 123.60 meters above sea level (MASL) was reached, just below the face of the dam. After that, there was a second flood of 7 700 m^3/s, reaching a height of 112.40 MASL, filling the enclosure between the dam, which caused a delay in the construction program of the Dam.

The aforementioned events left the following lessons and experiences in regards to the tunnels: 1) the importance of placing a fusible tunnel to safeguard the integrity of the dam; 2) the advantage of using hydraulic concrete only in the tunnels' floor which allows the return period to change from 164 to 188 years (Tr). Likewise, by changing to concrete in the walls and vault, the *Tr* can increase to 313 years, which represents a significant increase in the safety of the hydraulic, geological, and structural system, also allowing for significant savings. Out of this, the concept of "composite roughness" is born that can be implemented with a risk analysis for each instance of the tunnels' design.

Open Access bajo la licencia CC BY-NC-SA 4.0 (https://creativecommons.org/licenses/by-nc-sa/4.0/)

General aspects of composite roughness in tunnels or channels

No matter the shape of the subsections of the cross-section of a channel or tunnel (circular, trapezoidal, arch, horseshoe, etc.) when it comes to composite roughness, the main factor is the resistance coefficient ***n***, which can be combined in the floor, walls, and vault. This coefficient modifies the velocity distribution along the cross-section (Marengo, 2019), and for its study, several equations allow for the definition of its value homogeneously considering only the wetted perimeter (Marengo, & Arreguín, 2008). The study of the effects of varying the roughness on flow has been estimated through several types of analyses: physical, numerical, 2D, and three-dimensional models, as well as by on-site instrumentation combined with theoretical and empirical numerical analyses, which is the subject of study of the present research.

Flow resistance depends on four components (Rouse, 1965): 1) the friction layer, 2) drag, 3) deformation resistance and 4) resistance associated with flow instability. Then Weisbach's drag coefficient f, is a function (F) of:

$$f = F(\boldsymbol{Re}, k, \eta, N, F, U) \quad (1)$$

Open Access bajo la licencia CC BY-NC-SA 4.0 (https://creativecommons.org/licenses/by-nc-sa/4.0/)

Where: $\boldsymbol{Re}$ is the Reynolds number; k is the relative roughness, which is expressed as $ks/Rh\,k$, where ks is the equivalent of the wall surface roughness and Rh is the hydraulic radius; η is a function of the geometric shape of the cross-section; N is the uniformity number of the channel for both the contour and the plane; F is the Froude number, and U is the degree of instability of the flow. Rouse (1965) showed that the Moody diagram is a special case of Equation (1) for steady flow in rigid straight pipes of constant diameter by only considering two of the six independent parameters, which are: the Reynolds number and the relative roughness $ks/\boldsymbol{Re}$. The latter allows the calculation of Nikuradse roughness.

The formulas commonly used in open channels with a uniform flow to calculate the resistance coefficient are:

Manning's equation:

$$V = \frac{K_n}{n} Rh^{2/3} S_f^{1/2} \tag{2}$$

Homogeneous Manning's equation:

$$V = \frac{g^{1/2}}{n_g} Rh^{2/3} S_f^{1/2} \tag{3}$$

Open Access bajo la licencia CC BY-NC-SA 4.0 (https://creativecommons.org/licenses/by-nc-sa/4.0/)

Darcy-Weisbach Equation:

$$V = \left(\frac{2g}{f}\right)^{1/2} D^{1/2} \left(\frac{h_f}{L}\right)^{1/2} \tag{4}$$

Chézy equation:

$$V = C{R_h}^{1/2} S_f^{1/2} \tag{5}$$

Hazen Williams equation:

$$V = K_{HW} C_{HW} R^{0.63} S_f^{0.54} \tag{6}$$

Where V, is the average cross-sectional velocity; n, f, and C are the Manning, Weisbach, and Chézy drag coefficients, respectively; R_h is the hydraulic radius; S_f is the frictional slope; g is the acceleration of gravity. $K_n = 1m^{1/2}/s$.

And the resistance coefficients can be related using the above equations:

$$\sqrt{\frac{8}{f}} = \frac{C}{\sqrt{g}} = \frac{K_n}{\sqrt{g}} \frac{Rh^{1/6}}{n} \frac{Rh^{1/6}}{n_g} = \frac{V}{\sqrt{gRhS_f}} \tag{7}$$

Tecnología y ciencias del agua, ISSN 2007-2422, 13(2), DOI: 10.24850/j-tyca-2022-02-04

Open Access bajo la licencia CC BY-NC-SA 4.0 (https://creativecommons.org/licenses/by-nc-sa/4.0/)

According to Marengo (2019), in professional practice, the Manning equation is still used. In the case of a uniform flow and from the spatial point of view (Chow, 1959), the flow, hydraulic area, velocity and discharge in each section of the tunnel are constant, and the hydrostatic slope S_f, water surface S_w, and bottom of the channel S_0 are parallel, i.e.: $S_w = S_f = S_0$. And the denominator is called the shear velocity, V_*, which is defined as:

$$V_* = \sqrt{gRhS_f} \tag{8}$$

This allows the coefficient of friction C_f to be determined:

$$C_f = \left(\frac{V_*}{V}\right)^2 \tag{9}$$

According to Equation (9) and Equation (7), the following can be expressed:

$$C_f = \frac{f}{8} = \frac{g}{c^2} = \frac{g}{k_n^2}\frac{n^2}{R_h^{1/3}} = \frac{n_g^2}{R_h^{1/3}} \tag{10}$$

Tecnología y ciencias del agua, ISSN 2007-2422, 13(2), DOI: 10.24850/j-tyca-2022-02-04

Open Access bajo la licencia CC BY-NC-SA 4.0 (https://creativecommons.org/licenses/by-nc-sa/4.0/)

When considering various roughness materials, for example, hydraulic concrete in floor and walls and shotcrete in the vault, or rock, the value of n, from Equation (2), an equivalent coefficient must be obtained and this could change with the water level (Marengo, 2019).

Experimental design

Instrumentation for measuring hydraulic variables

Geometric and hydraulic characteristics of tunnels

The research is centered on the case study of the communication tunnels of the upper and lower Grijalva River, upstream of the Penitas Dam (Angel Albino Corzo), with the characteristics mentioned below.

It consists of two tunnels (T1 and T2) located on the left bank of the Grijalva River, with an arch section of 14 m wide by 14 m high and a

Tecnología y ciencias del agua, ISSN 2007-2422, 13(2), DOI: 10.24850/j-tyca-2022-02-04

Open Access bajo la licencia CC BY-NC-SA 4.0 (https://creativecommons.org/licenses/by-nc-sa/4.0/)

horizontal hydraulic concrete floor and walls, and a vault of shotcrete (Table 1). Both channels contribute to the regulation of the operation between the two dams Malpaso and Penitas (Table 2).

Table 1. Geometric characteristics of the tunnels.

Tunnel 1 and 2		
Design flow rate	2 604.00	m^3/s
Return period	1 0000	years
Reservoir level	105.99	m
Tunnel 1 length	1 200.96	m
Tunnel 2 length	1 187.04	m
Slope	Horizontal	-
Elevations at outlet and inlet	76.50	m
Arch section	14x14	m
Vault radius	7.00	m

Table 2. Operating Levels of Penitas and Malpaso Dams.

Peñitas Dam	
NAME Elevation	95.50 m
NAMO Elevation	87.40 m
NAMINO Elevation	85.00 m

Open Access bajo la licencia CC BY-NC-SA 4.0 (https://creativecommons.org/licenses/by-nc-sa/4.0/)

Superior elevation of spillway gates	91.14 m
Generation units	4.00
Flow rate by the generation unit	349.00 m³/s
Malpaso Dam	
Elevation of outlet	86.50 m
Generation units	6.00
Flow rate by the generation unit	240.00 m³/s

Instrumentation installation

A hydraulic instrumentation project was carried out consisting of installing 53 hydrostatic pressure sensors (measuring cells), programmed to measure water levels. Each tunnel has 24 sensors spaced out at a distance of 50 m of one another (in each tunnel), as well as 5 additional ones along each of the entrance and exit portals (Figure 2).

Tecnología y ciencias del agua, ISSN 2007-2422, 13(2), DOI: 10.24850/j-tyca-2022-02-04

Open Access bajo la licencia CC BY-NC-SA 4.0 (https://creativecommons.org/licenses/by-nc-sa/4.0/)

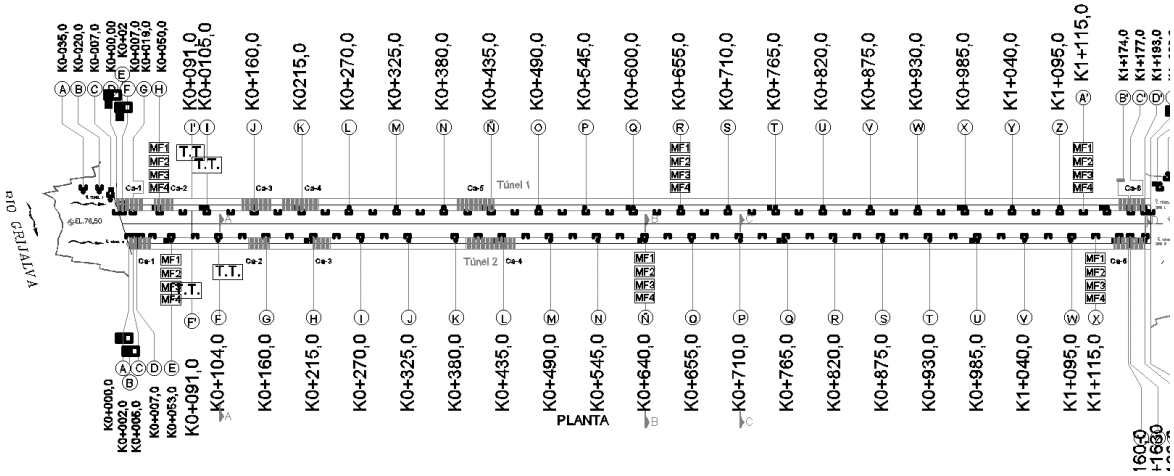

Figure 2. Location of cells in the Tunnels (Tunnel 1 above and Tunnel 2 below in the Figure).

The sensors are of the "vibrating wire" type, which is installed in the concave part of the concrete that joins the wall with the template in the cross-section of the tunnel, this area is known as "chamfer" (Figure 3). The sensors contain a vibrating wire or cable that detects the hydraulic pressure using a diaphragm, which transforms the resonance frequency into a hydraulic pressure value and in turn, into a water level value. The sensors are previously calibrated in the laboratory and the programming is done in the SCADA system to transform it into values of hydrostatic pressure or hydraulic levels in meters above sea level (MASL).

Open Access bajo la licencia CC BY-NC-SA 4.0 (https://creativecommons.org/licenses/by-nc-sa/4.0/)

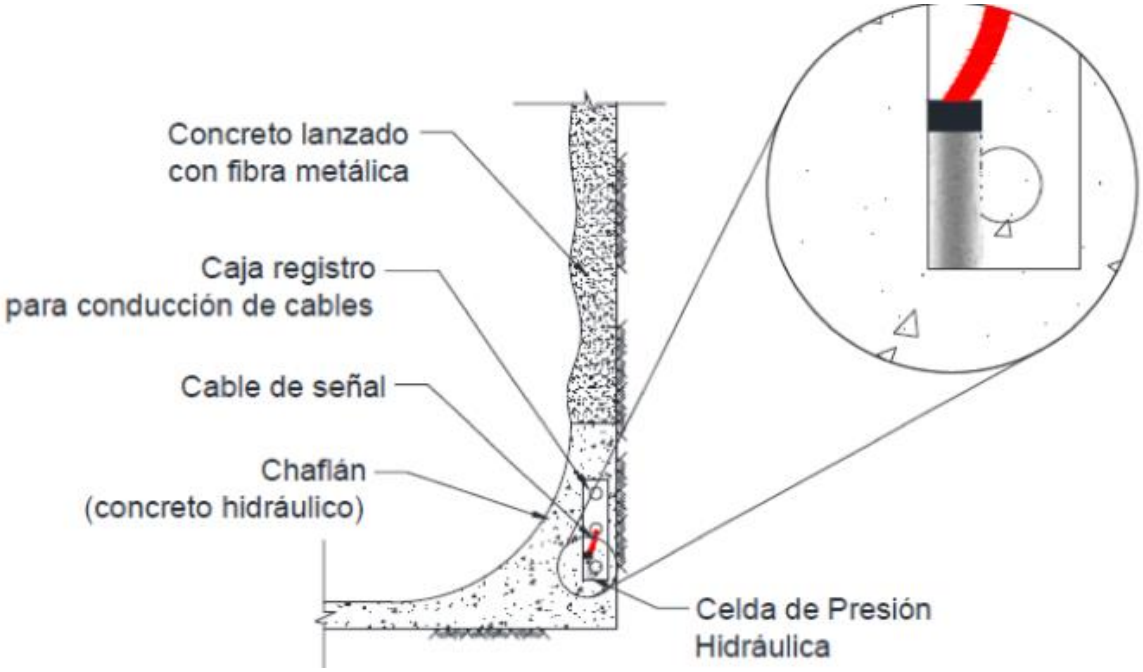

Figure 3. Placement of cells within the "chamfer".

For flow water, one module of Doppler equipment of the "Time in Traverse (T.T.)" type was installed per tunnel on the walls. Each module is located between sections 0+091 and 0+105 (Figure 4), which kept the local effect of the inlet from having an influence. The module consists of four pairs (eight sensors) measuring at different heights: 2.5 m, 5 m, 6.5 m, and 8 m (Figure 5). It works for a velocity range of +-20 m/s and channels with a width of 0.75 m to 100 m and a minimum to a maximum range of temperatures varying from -20 °C to +70 °C and with an accuracy variation of only 0.5 %.

Open Access bajo la licencia CC BY-NC-SA 4.0 (https://creativecommons.org/licenses/by-nc-sa/4.0/)

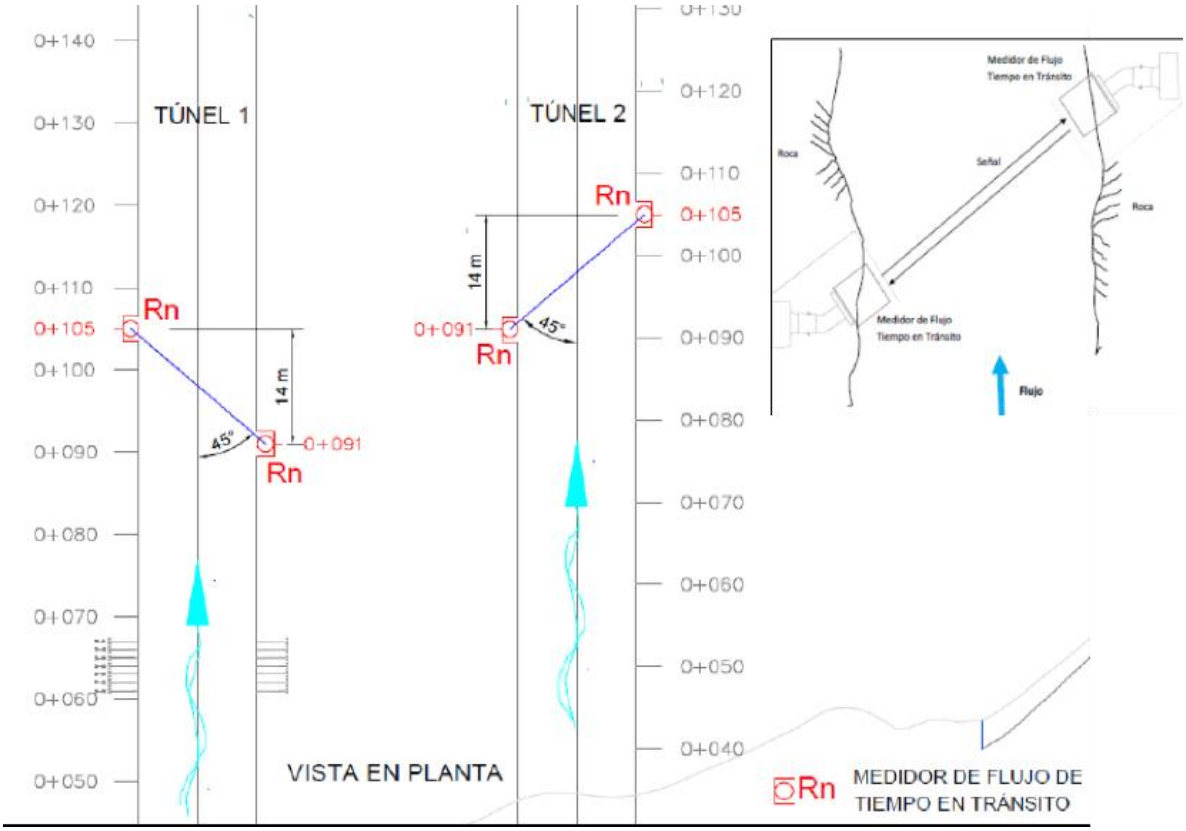

Figure 4. Location of "Time in traverse" meters (in the plant).

Tecnología y ciencias del agua, ISSN 2007-2422, 13(2), DOI: 10.24850/j-tyca-2022-02-04

Open Access bajo la licencia CC BY-NC-SA 4.0
(https://creativecommons.org/licenses/by-nc-sa/4.0/)

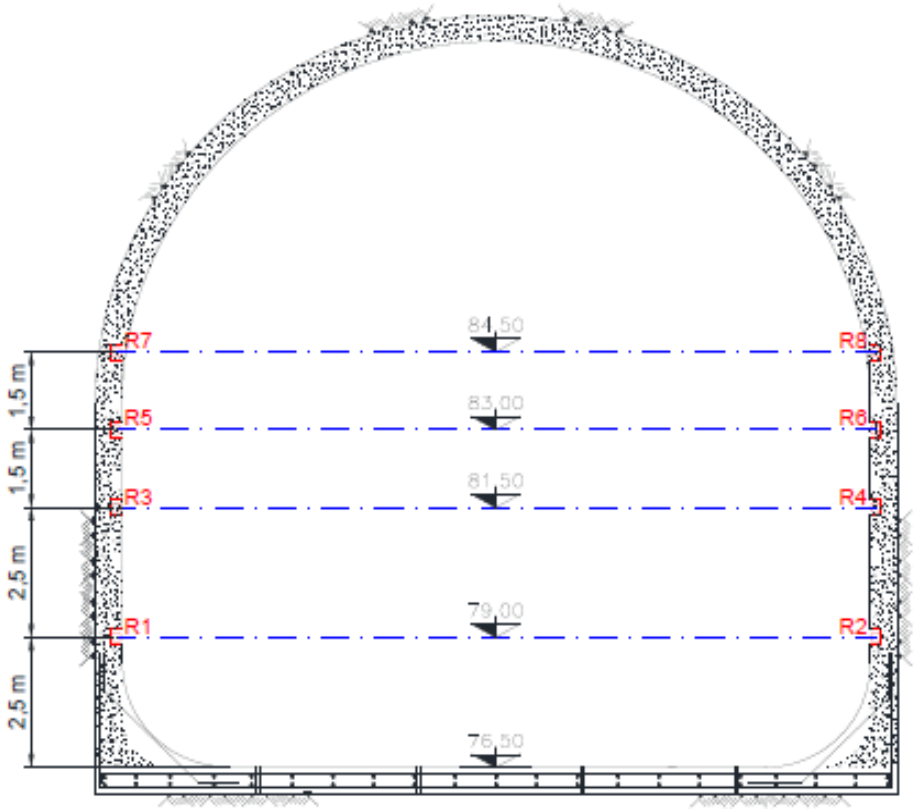

Figure 5. Location of "Time in Traverse" gauges (in profile or section).

The T.T. concept is because the equipment sends a sound beam to another instrument installed at 45 degrees at the same elevation on the opposite wall, measuring in each pair the time it takes to return from downstream to upstream, thus calculating the fluid velocity. Water has small amounts of particles so the operation of T.T. meters is favored.

To measure velocities, close to the wall, four doppler modules were installed. They have a higher frequency (3000 kHz), which allows them to measure velocities from 0.1 m to 5.0 m distance from the wall. Each piece of equipment has two sensors at 25º, which gives redundancy to the

Tecnología y ciencias del agua, ISSN 2007-2422, 13(2), DOI: 10.24850/j-tyca-2022-02-04

Open Access bajo la licencia CC BY-NC-SA 4.0 (https://creativecommons.org/licenses/by-nc-sa/4.0/)

measurement. They were placed in three sections of each tunnel: K0+050, K0+655, and K1+115 (Figure 6), and at different heights: 2.5, 5, 6.5, and 8 m (Figure 7), to measure a general spectrum in the section. Each piece of equipment was programmed to measure from 10 cm to 1.5 m away from the wall because the objective was to measure in the zone of influence of the wall, this had an accuracy variation of only 0.1 % and measures at depths of up to 30 m. Its velocity ranges up to 6 m/s.

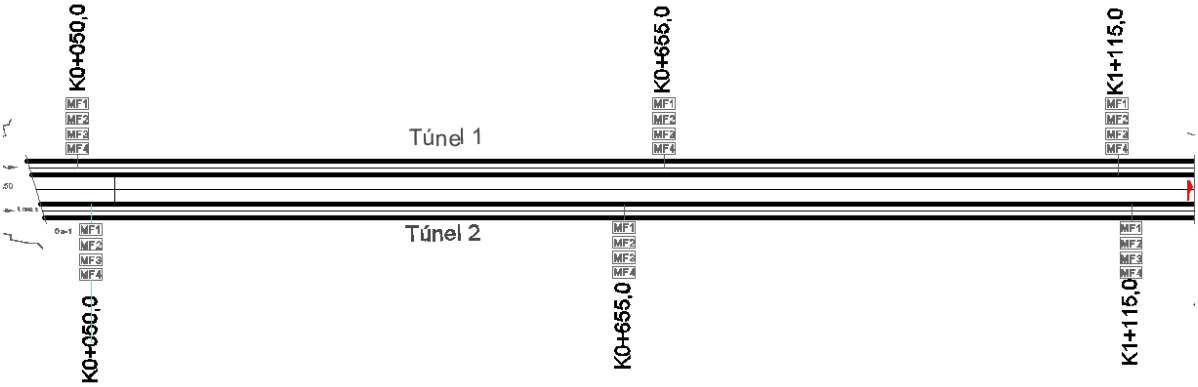

Figure 6. Location of Doppler velocity meters (in the plant).

Tecnología y ciencias del agua, ISSN 2007-2422, 13(2), DOI: 10.24850/j-tyca-2022-02-04

Open Access bajo la licencia CC BY-NC-SA 4.0 (https://creativecommons.org/licenses/by-nc-sa/4.0/)

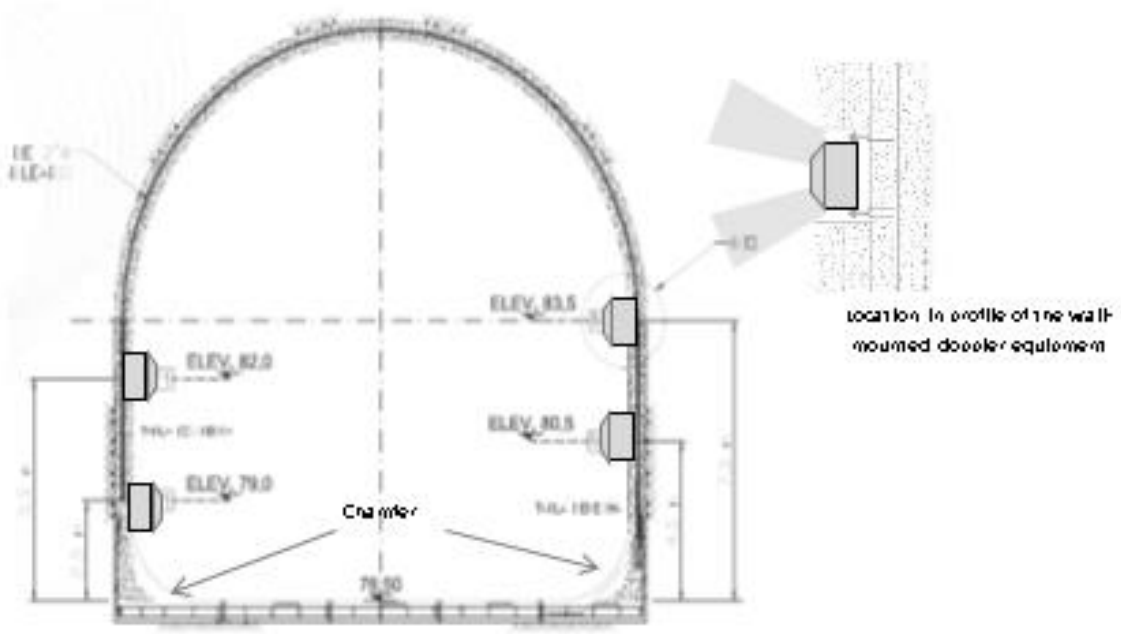

Figure 7. Location of Doppler velocity meters (in section).

Gauging campaign at the inlet portal

To verify the certainty of the hydraulic variables, a gauging campaign was carried out in the inlet portal of the tunnels (Figure 1). It was compared with the flow rate of the T.T. meters installed inside the tunnel. A Doppler moving profiler (ADCP) was used for gauging, it had the following

Tecnología y ciencias del agua, ISSN 2007-2422, 13(2), DOI: 10.24850/j-tyca-2022-02-04

Open Access bajo la licencia CC BY-NC-SA 4.0 (https://creativecommons.org/licenses/by-nc-sa/4.0/)

characteristics: a depth varying from 75 cm to 30 m; an accuracy variation of 0.5 %; velocities of +-20m/s; and a temperature range of -5 °C to +45 °C.

Flow water rate approximations were obtained from the ADCP movable Doppler for the T.T. meter ranging from -3 to 8 %. This difference is acceptable upon adding the tolerances of both pieces of equipment. Therefore, it was concluded that the T.T. meter installed inside the tunnels gives a better quality of instantaneous measurement in each reading: its configuration is designed to adjust with the other pairs of meters in case one of them is missing; it has a 0.5 % absolute error margin. Also, hydraulic parameters obey the fundamental theories and laws of fluid mechanics applied to the distribution of velocities in a rough bottom channel.

Methodology

Part 1. A theoretical approach to the calculation of the Manning's composite roughness, n_c

Open Access bajo la licencia CC BY-NC-SA 4.0
(https://creativecommons.org/licenses/by-nc-sa/4.0/)

Once the quality of the flow and the velocity measurement data has been verified, we proceed with the theoretical approach for the calculation of the composite roughness n_c, starting with Bernoulli's Equation and Manning's Equation (Sotelo, 2002), where we know all the variables except for the roughness (Figure 8).

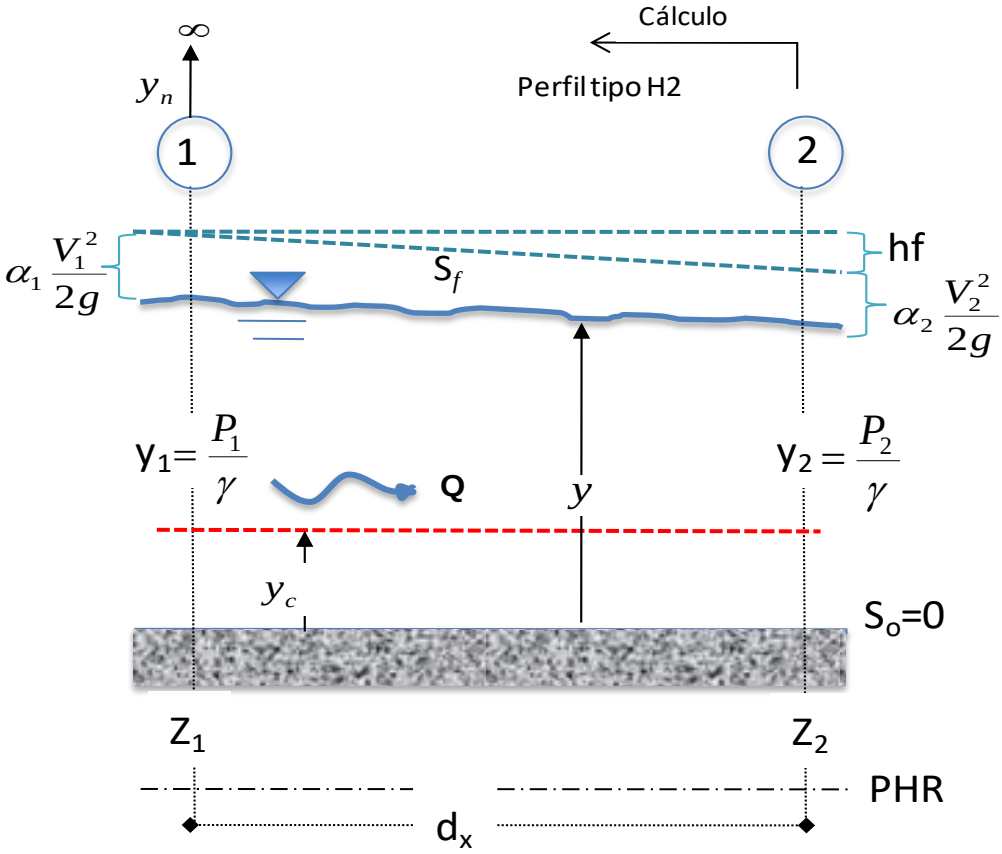

Figure 8. Hydraulic calculation approach for roughness estimation.

Tecnología y ciencias del agua, ISSN 2007-2422, 13(2), DOI: 10.24850/j-tyca-2022-02-04

Open Access bajo la licencia CC BY-NC-SA 4.0 (https://creativecommons.org/licenses/by-nc-sa/4.0/)

If we only do not know the friction losses, h_f:

$$h_f = \int_1^2 S_f \, dx = \int_1^2 \frac{Q^2 {n_c}^2}{A^2 {R_h}^{4/3}} dx \approx \frac{\Delta x}{2} {n_c}^2 Q^2 \left(\frac{1}{A_1^2 {R_{h_1}}^{4/3}} + \frac{1}{A_2^2 {R_{h_2}}^{4/3}} \right) \quad (11)$$

Where S_f, is the friction slope; A, is the hydraulic area; R_h, is the hydraulic radius; k_l is the local loss coefficient if any; $y_1 - y_2$ is the difference in hydraulic levels in a section as seen in Figure 8; and Q, the flow is known. By subtracting the composite roughness in the n_c section. From Eq. 11, it follows that:

$$n_c = \left[\frac{2(y_1 - y_2) + \frac{Q^2}{g}\left(\frac{1}{A_1^2} - \frac{1}{A_2^2} - \frac{k_l}{A_2^2}\right)}{Q^2 \Delta x \left(\frac{1}{A_1^2 {Rh_1}^{4/3}} + \frac{1}{A_2^2 {Rh_2}^{4/3}} \right)} \right]^{1/2} \quad (12)$$

Where:

$$\Delta x = (x_2 - x_1) \quad (13)$$

The roughness is composed of hydraulic concrete in the floor and chamfer and shotcrete in walls and vault (Figure 9).

Tecnología y ciencias del agua, ISSN 2007-2422, 13(2), DOI: 10.24850/j-tyca-2022-02-04

Open Access bajo la licencia CC BY-NC-SA 4.0 (https://creativecommons.org/licenses/by-nc-sa/4.0/)

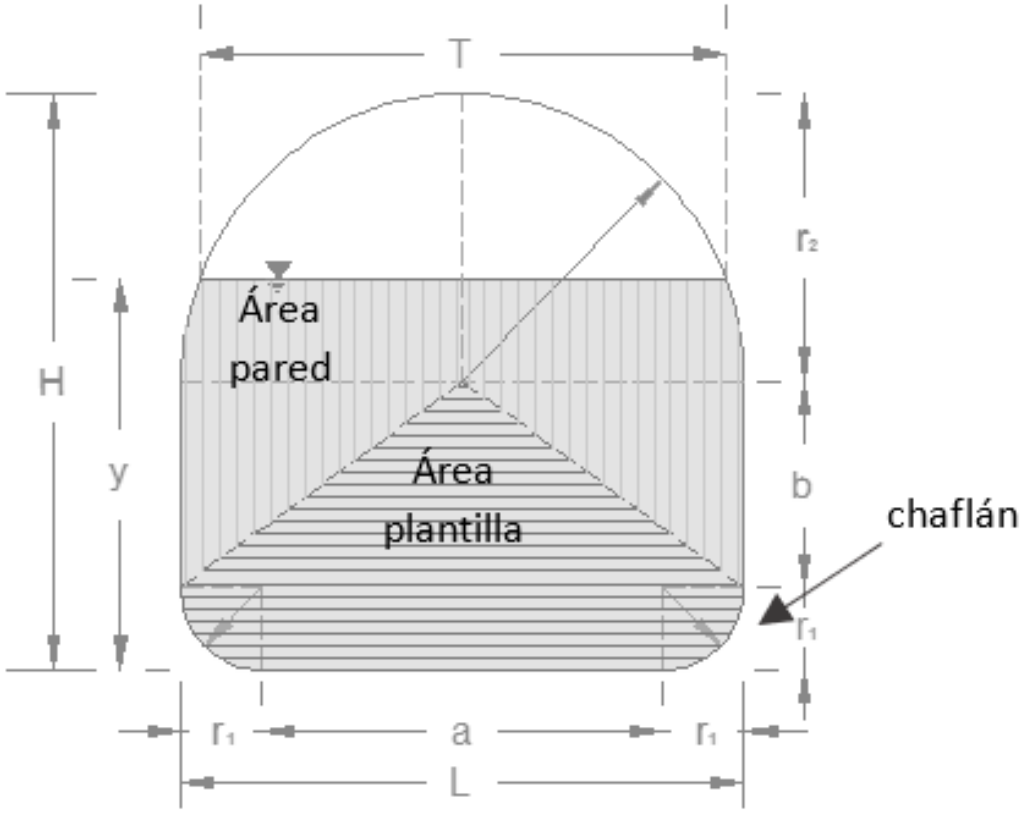

Figure 9. Portal section with composite roughness.

Once the roughness values n_c are obtained for each section, the discretization of the equivalent Nikuradse roughness k_s is carried out to obtain the real wall and floor roughness value.

Part 2. Equivalent Nikuradse roughness estimation

Tecnología y ciencias del agua, ISSN 2007-2422, 13(2), DOI: 10.24850/j-tyca-2022-02-04

Open Access bajo la licencia CC BY-NC-SA 4.0 (https://creativecommons.org/licenses/by-nc-sa/4.0/)

Prandtl and Von Kármán's logarithmic law of velocities

The logarithmic law by Prandtl and Von Kármán establish that the velocity profile near the wall or in the boundary layer zone can be expressed as follows (Schlichting, 1979):

$$\frac{\overline{v}}{v_*} = \frac{1}{\kappa} ln \frac{y}{k_s} + B \tag{14}$$

Where $\overline{v}$ represents the Reynolds-averaged longitudinal velocity; v_* the fluid velocity in the zone of influence of the wall; y the distance to the wall; κ=0.4 the Von Kármán constant; k_s the Nikuradse equivalent roughness and $B = 8.5$ correspond to the rough bottom channels. Therefore Equation (4) for completely rough channels is as follows:

$$\frac{\overline{v}}{v_*} = 2.5\, ln \frac{y}{k_s} + 8.5 \tag{15}$$

There are three conditions for determining the constant B, which depends on the Reynolds number, in terms of $v_* k_s / v$, where it is equal to 5 for completely smooth walls; 5 to 70 corresponds to the transition from

Tecnología y ciencias del agua, ISSN 2007-2422, 13(2), DOI: 10.24850/j-tyca-2022-02-04

Open Access bajo la licencia CC BY-NC-SA 4.0 (https://creativecommons.org/licenses/by-nc-sa/4.0/)

a hydraulically smooth to a completely rough regime; and greater than 70 for completely rough flow (Schlichting, 1979) (Figure 10).

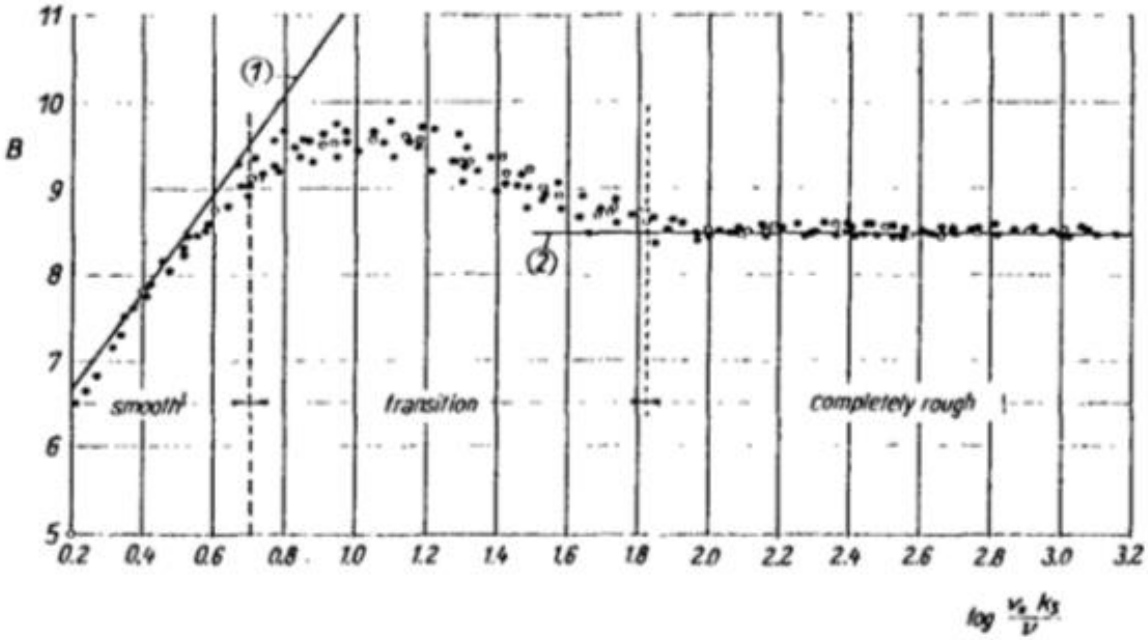

Figure 10. Function B for roughness in terms of $v_* k_s / v$, for Nikuradse sand roughness (Schlichting, 1979).

Boundary layer and displacement thickness

Tecnología y ciencias del agua, ISSN 2007-2422, 13(2), DOI: 10.24850/j-tyca-2022-02-04

Open Access bajo la licencia CC BY-NC-SA 4.0 (https://creativecommons.org/licenses/by-nc-sa/4.0/)

Boundary layer of a flow is the zone in which the fluid motion dominantly experiences the braking effect caused by the presence of the wall. The concept of a no-slip boundary condition is due to L. Prandtl.

It can also be described as the necessary thickness at which the wall has to be displaced to make the volume lost equal to the volume lost due to the viscous effect of the wall (Figure 11). The vertical displacement is called "displacement thickness", and is defined as:

$$\delta^* = \int_0^{\delta} (1 - \frac{\overline{v}}{v}) \mathrm{dy} \qquad (16)$$

Where $\overline{v}$ is the longitudinal velocity of the flow at a distance from the surface and the wall, measured perpendicular to the wall, and v is the velocity outside the boundary layer.

Tecnología y ciencias del agua, ISSN 2007-2422, 13(2), DOI: 10.24850/j-tyca-2022-02-04

Open Access bajo la licencia CC BY-NC-SA 4.0 (https://creativecommons.org/licenses/by-nc-sa/4.0/)

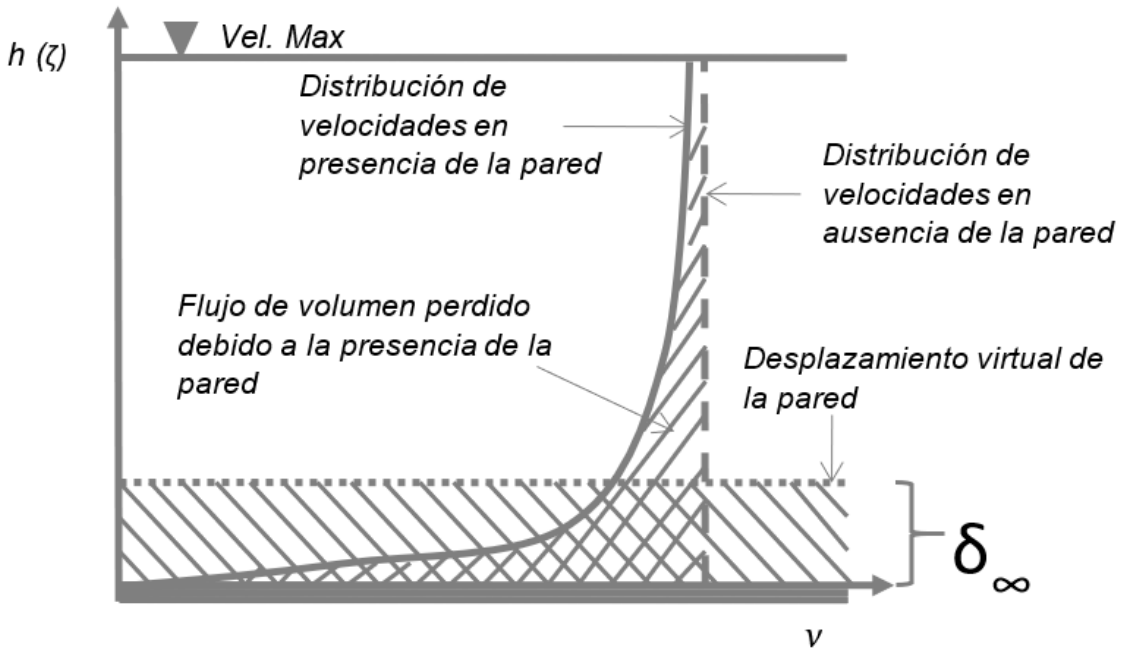

Figure 11. Interpretation of displacement thickness.

The value of the displacement thickness δ^* usually varies from one-tenth of the boundary layer thickness onward, according to the magnitude of the Reynolds number, where small viscosity ranges are large Reynolds numbers.

The velocity profile in the boundary layer

Tecnología y ciencias del agua, ISSN 2007-2422, 13(2), DOI: 10.24850/j-tyca-2022-02-04

Open Access bajo la licencia CC BY-NC-SA 4.0 (https://creativecommons.org/licenses/by-nc-sa/4.0/)

Considering the above, the experimental methodology was proposed based on the Doppler velocity recordings for velocities from 10 cm up to 2.1 m distance from the wall and with measurement segments every 20 cm.

First, it is necessary to verify if the recorded velocities are within the displacement thickness, δ_d, through the following equation:

$$\delta d = \left\{1 - \left[e^{-kB}\frac{ks}{h} + \frac{ln\frac{h}{ks}+Bk-1}{ln\frac{h}{ks}+Bk}\right]\right\}h \qquad (17)$$

Where, δd, is the displacement thickness; $\kappa = 0.4$ the Von-Kármán constant; $B = 8.5$ for rough bottom channels; k_s the Nikuradse equivalent roughness; h is the mean value of the section strain.

Each velocity recorded by the Doppler sensor considers different distances along the length of the displacement thickness that generates different velocity profiles along with the influence of the boundary layer and the displacement thickness. Values that develop as logarithmic velocity curves are considered.

Nikuradse equivalent roughness, *ks*

Tecnología y ciencias del agua, ISSN 2007-2422, 13(2), DOI: 10.24850/j-tyca-2022-02-04

Open Access bajo la licencia CC BY-NC-SA 4.0 (https://creativecommons.org/licenses/by-nc-sa/4.0/)

Equivalent Nikuradse roughness is obtained from Equation (5), where parameter $\boldsymbol{k_s}$ from logarithmic law regards:

$$k_s = e^{\left(kB - \frac{\beta}{v_*}\right)} \tag{18}$$

where:

$$\beta = \bar{v}_2 - \left(\frac{\bar{v}_2 - \bar{v}_1}{\eta_2 - \eta_1}\right)\eta_2 \tag{19}$$

$$\eta = ln\,\zeta = ln\ \ y \tag{20}$$

β defines the average velocities from the first measurement reading, ranging from 10 to 30 cm and afterward 20 cm every segment. Thus $\bar{v}_2 - \bar{v}_1$ refers to the velocity value obtained with the sensor at 30 cm ($\bar{v}_2$) and at 10 cm ($\bar{v}_1$); $\eta = ln\,\zeta = ln\ \ y$, where y is the distance in regards to the wall from the sensor (at 10 and 30 cm).

And the velocity in the wall region (v_*) is defined as:

$$v_* = \alpha = \frac{\bar{v}_2 - \bar{v}_1}{\eta_2 - \eta_1} \tag{21}$$

Tecnología y ciencias del agua, ISSN 2007-2422, 13(2), DOI: 10.24850/j-tyca-2022-02-04

Open Access bajo la licencia CC BY-NC-SA 4.0 (https://creativecommons.org/licenses/by-nc-sa/4.0/)

Once the equivalent roughness k_s is obtained, it is possible to calculate the value of the parameter f, known as Nikuradse's f.

According to Aldama and Ocón (2002) in channels with uniform flow $S_f = S$, a relationship can be found between the Manning and Darcy-Weisbach formulas. Therefore the following expression relates the roughness factor (n) to the dimensionless friction factor (f):

$$n = (f/8g)^{1/2} Rh^{1/6} \tag{22}$$

Likewise, in a flat bottom made up of sand grains, the roughness n is proportional to the diameter of these grains raised to 1/6 (Aldama, & Ocón, 2002), which results in the following equation:

$$n = k_m g^{-1/2} ks^{1/6} \tag{23}$$

Where k_m is a dimensionless constant equal to 0.129765776 (Aldama & Ocón, 2012). Likewise, considering for wide channels $R=h$ and clearing f we obtain:

$$f = 8{k_m}^2 (ks/Rh)^{1/3} \tag{24}$$

Open Access bajo la licencia CC BY-NC-SA 4.0 (https://creativecommons.org/licenses/by-nc-sa/4.0/)

According to Aldama and Ocón (2002), the graphs for the friction factor f corresponding to circular ducts working at full or half full and wide channels produce values that do not exceed more than a 5 % difference, so the applicability of the above equations can be included.

For the present study, that same procedure is being considered, using input values obtained from the composite roughness of Equation (12) and for the sections where the doppler meters are located (K0+050, K0+655, and K1+115).

Likewise, those are within the hydraulic concrete roughness intervals between 0.012 and 0.019 and shotcrete between 0.020 and 0.028 (Marengo & Arreguín, 2008). Those within the displacement thickness are also considered, that is, the velocity profile of each of the records is reviewed: only those that fit the logarithmic distribution of velocities along the entire length of the displacement thickness are chosen.

Part 3. One-dimensional theoretical model and calibration of results with application to 18 empirical composite roughness equations

2022, Instituto Mexicano de Tecnología del Agua

Open Access bajo la licencia CC BY-NC-SA 4.0 (https://creativecommons.org/licenses/by-nc-sa/4.0/)

Once the wall roughness parameters (Equation (22)) have been obtained, and the composite roughness is known from the Energy equation (Equation (12)), then each of the 17 known empirical composite roughness equations (Table 3) must be applied to obtain the roughness parameter that best approximates to measurements.

Table 3. Empirical equations for estimating the resistance coefficient n_c in channels with composite roughness (Marengo & Arreguín, 2008).

		Assumptions	
Eqs	n_c	**Concept**	**Equation**
A	$=\frac{\sum n_i A_i}{A}$	Sum of component n weighted by area ratio; or Total shear velocity is a weighted sum of subarea shear velocity	$\sqrt{gRS}=\sum\left(\frac{P_i}{P}\sqrt{gR_iS_i}\right)$ $(V_i/V)=(R_i/R)^{7/6}$
B	$=\sqrt{\sum n_i^2\frac{A_i}{A}}$	Total resistance force is equal to the sum of subarea resistance forces; or, n_i weighted by √Ai Total discharge is the sum of subarea discharges	$P\gamma RS=\Sigma P_i\gamma R_iS_i$ $(V_i/V)=(R_i/R)^{2/3}$
C	$=\frac{A}{\sum(A_i/n_i)}$	Total discharge is the sum of subarea discharges	$Q=VA=\Sigma(V_iA_i)\Sigma Q_i$ $(S_i/S)=(R/R_i)^{4/3}$
D	$=\left[\frac{\sum(n_i^{3/2}A_i)}{A}\right]^{2/3}$	Same as Horton and Einstein´s Eq. E but derived erroneously	
E	$=\left[\frac{1}{P}\sum\left(n_i^{3/2}P_i\right)\right]^{2/3}$	Total cross-sectional mean velocity equal to subarea mean velocity	$V=V_i$ $A=\Sigma A_i$ $S=S_i$

Open Access bajo la licencia CC BY-NC-SA 4.0 (https://creativecommons.org/licenses/by-nc-sa/4.0/)

		Assumptions	
Eqs	n_c	**Concept**	**Equation**
F	$= \frac{P}{\sum(P_i/n_i)}$	Total discharge es the sum of subarea discharges	$Q = \Sigma Q_i$ $(S_i/S) = (R/R_i)^{10/3}$
G	$= \left[\frac{1}{P}\sum(n_i^2 P_i)\right]^{1/2}$	Total resistance force, F, is the sum of subarea resistance forces, ΣFi	$P\gamma RS = \sum P_i \gamma R_i S_i$ $(V_i/V) = (R_i/R)^{1/6}$
H	$= \frac{\sum(n_i P_i)}{P}$	Total shear velocity is a weighted sum of subarea shear velocity; or, contributing component roughness is linearly proportional to the wetted perimeter	$\sqrt{gRS} = \sum\left(\frac{P_i}{P}\sqrt{gR_iS_i}\right)$ $(V_i/V) = (R_i/R)^{1/6}$ *or* $n_c P = \sum(n_i P_i)$
I	$= \left[\frac{R^{1/3}}{P}\sum\frac{n_i^2 P_i}{R_i^{1/3}}\right]^{1/2}$	Total resistance force, F, is the sum of subarea resistance forces, ΣFi	$P\gamma RS = \sum P_i \gamma R_i S_i$ $(V_i/V) = 1$
J	$= \left[\frac{\sum n_i^2 P_i R_i^{2/3}}{PR^{2/3}}\right]^{1/2}$	Total resistance force equal to the sum of subareas resistance forces	$P\gamma RS = \sum P_i \gamma R_i S_i$ $(V_i/V) = (R_i/R)^{1/2}$
K	$= \frac{PR^{7/6}}{\sum\frac{P_i}{n_i}R_i^{7/6}}$	Total discharge is the sum of subarea discharges	$Q = VA = \Sigma(V_i A_i)$ $(S_i/S) = (R/R_i)$
L	$= \frac{PR^{5/3}}{\sum\frac{P_i R_i^{5/3}}{n_i}}$	Total discharge is the sum of subarea discharges	$Q = VA = \Sigma(V_i A_i)$ $(S_i/S) = 1$ $R = A/P$
M	$= \frac{\sum P_i R_i^{5/3}}{\sum\frac{P_i R_i^{5/3}}{n_i}}$	Same as Eq. L with a modified definition of R	$Q = VA = \Sigma(V_i A_i)$ $(S_i/S) = 1$ ***R*** de $\frac{PR^{5/3}}{\sum P_i R_i^{5/3}} = \frac{AR^{2/3}}{\sum A_i R_i^{2/3}} = 1$

Tecnología y ciencias del agua, ISSN 2007-2422, 13(2), DOI: 10.24850/j-tyca-2022-02-04

Open Access bajo la licencia CC BY-NC-SA 4.0 (https://creativecommons.org/licenses/by-nc-sa/4.0/)

		Assumptions	
Eqs	n_c	**Concept**	**Equation**
N	$= \frac{\sum\left(n_i P_i / R_i^{1/6}\right)}{P / R^{1/6}}$	Total shear velocity, $\sqrt{\mathrm{gRS}}$ is a weighted sum of subarea shear velocity	$\sqrt{gRS} = \sum\left(\frac{P_i}{P}\sqrt{gR_iS_i}\right)$ $(V_i/V) = 1$
O	$= \frac{\sum\left(n_i P_i R_i^{1/2}\right)}{PR^{1/2}}$	Total shear velocity is a weighted sum of subarea shear velocity	$\sqrt{gRS} = \sum\left(\frac{P_i}{P}\sqrt{gR_iS_i}\right)$ $(V_i/V) = (R_i/R)^{2/3}$
P	$= \frac{\sum\left(n_i P_i R_i^{1/3}\right)}{PR^{1/3}}$	Total shear velocity is a weighted sum of subarea shear velocity	$\sqrt{gRS} = \sum\left(\frac{P_i}{P}\sqrt{gR_iS_i}\right)$ $(V_i/V) = (R_i/R)^{1/2}$
Z	$= exp\left[\frac{\sum P_i h_i^{3/2} ln \quad n_i}{\sum P_i h_i^{3/2}}\right]$	Logarithmic velocity distribution over depth h for wide channel	$S = S_i\,,\, Q = \sum Q_i$ $\frac{Q_i}{2.5\sqrt{gS}} = h_i^{\frac{3}{2}} P_i \left[ln\left(\frac{10.93h_i}{k_i}\right)\right]$ $\frac{Q_i}{2.5\sqrt{gS}} = \Sigma h_i^{3/2} P_i \left[ln\left(\frac{1093h_i}{k_i}\right)\right]$ $n = 0.0342k$

This is achieved with a one-dimensional theoretical model that takes these equations and calibrates the logs. The one-dimensional theoretical model has the roughness coefficient of the shotcrete n_{cl} as a variable. In this case of a horizontal H2 profile, the control section is located downstream, and the equation that solves it is:

$$F(y) = \underbrace{Z_S - Z_{S-1} + Y_S + \frac{Q^2}{{A_S}^2 2g}(1+kl) + \frac{Q^2 n^2}{{A_S}^2 R {h_S}^{4/3}} \cdot \frac{\Delta x}{2}}_{know\ (Ys)} \qquad (25)$$

Tecnología y ciencias del agua, ISSN 2007-2422, 13(2), DOI: 10.24850/j-tyca-2022-02-04

Open Access bajo la licencia CC BY-NC-SA 4.0 (https://creativecommons.org/licenses/by-nc-sa/4.0/)

$$\underbrace{= Y_{S-1} + \frac{Q^2}{{A_{S-1}}^2 2g} - \frac{Q^2 n^2}{{A_{S-1}}^2 R {h_{S-1}}^{4/3}} \cdot \frac{\Delta x}{2}}_{unknown \quad (Ys-1)}$$

It is a quasi-permanent model because it is analyzed with flow records, and the theories for a gradually varying flow are applied.

The model starts from a known downstream value, the head is measured by a sensor. Once the flow is known, there is a unique relationship for obtaining the geometric variables such as area, perimeter, and hydraulic radius, that were previously defined by their corresponding formula. Flow, wall, and floor roughness obtained from the direct measurements of the Doppler meters are introduced as variables for each case. This scheme is applied to 17 known empirical equations to estimate composite roughness (Table 3). That allows for the construction of a hydraulic profile that will be adjusted with the profile of measured level values from sensors.

To select the best adjustment equation, the concept of the Minimum Square Error (MSE) is used. Then composite roughness obtained in the measurement of Doppler sections is used through Bernoulli and Manning Equation (Equation (12)) and is compared with the composite roughness obtained with the 17 empirical equations. In both of them, wall and floor point roughness obtained with Doppler equipment were integrated (Equations (18) to (24)). With the above, the MSE obtained will allow defining the best-adjusted Equation among the 17 known ones or defining a new equation.

Tecnología y ciencias del agua, ISSN 2007-2422, 13(2), DOI: 10.24850/j-tyca-2022-02-04

Open Access bajo la licencia CC BY-NC-SA 4.0 (https://creativecommons.org/licenses/by-nc-sa/4.0/)

Results

Measurement of hydraulic variables

Hydraulic levels were programmed to be measured with the sensors every hour, and values from 8.72 to 10.66 m of water level were obtained.

The velocities measured with the Doppler equipment 10 cm from the wall and onward, had velocity ranges from 0.35 to 2.5 m/s. However, there were constant communication problems with the velocity equipment in Tunnel 2, therefore only the information from Tunnel 1 was considered for the roughness study.

The flows from Doppler "time in traverse" equipment in both tunnels (QT1+QT2) ranged from 117 to 575 m^3/s, between October 2011 and February 2012.

Tecnología y ciencias del agua, ISSN 2007-2422, 13(2), DOI: 10.24850/j-tyca-2022-02-04

Open Access bajo la licencia CC BY-NC-SA 4.0 (https://creativecommons.org/licenses/by-nc-sa/4.0/)

Composite roughness from Bernoulli and Manning's equations, Equation (1) and Equation (2)

The roughness values obtained for each analysis section are shown in the following graph (Figure 12), and only those within the recommended ranges were considered: hydraulic concrete between 0.012 and 0.019 and shotcrete between 0.020 and 0.028 (Marengo & Arreguín, 2008).

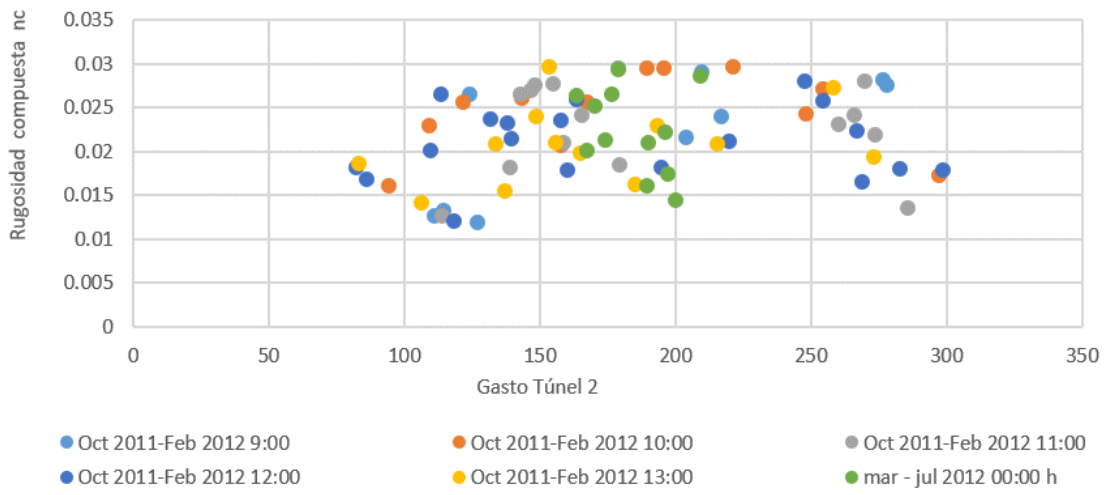

Figure 12. Composite roughness values were obtained from Equation (2) and within the recommended range (Marengo & Arreguín, 2008).

Tecnología y ciencias del agua, ISSN 2007-2422, 13(2), DOI: 10.24850/j-tyca-2022-02-04

Open Access bajo la licencia CC BY-NC-SA 4.0 (https://creativecommons.org/licenses/by-nc-sa/4.0/)

Nikuradse equivalent roughness (k_s), Equation (8), and displacement thickness (δd), Equation (7)

Velocities registered from Doppler equipment in sections K0+050 and K1+115 were modeled. No information could be extracted from the equipment located at K0+655. Measurements were scheduled every hour from October 2011 to October 2012. Each section had 4 pieces of Doppler equipment (Figure 6 and Figure 7) and they were programmed with the other measurement equipment: the modular equipment for flow and the sensors for measuring hydraulic levels.

Some complications encountered were that there was not always a constant measurement from all the equipment for all the time intervals. Also, during the rainy season there was constant damage to the transmission, due to the overloads that occurred in the instrumentation hut, where the SCADA systems were located. This led to continuous repairs throughout that time. Due to the inability to maintain the upkeeping, it was no longer possible to continue with the analysis of the data in the tunnels for more data in major conditions.

More than 200 velocity profiles were obtained for each measurement interval, from 1h to 24 h, in 1 year of measurement.

Those records belonging to a logarithmic profile were selected, totaling more than 300 profiles between 117 and 575 m^3/s of flow as shown in the following graphs (Figure 13, Figure 14, and Figure 15).

Open Access bajo la licencia CC BY-NC-SA 4.0 (https://creativecommons.org/licenses/by-nc-sa/4.0/)

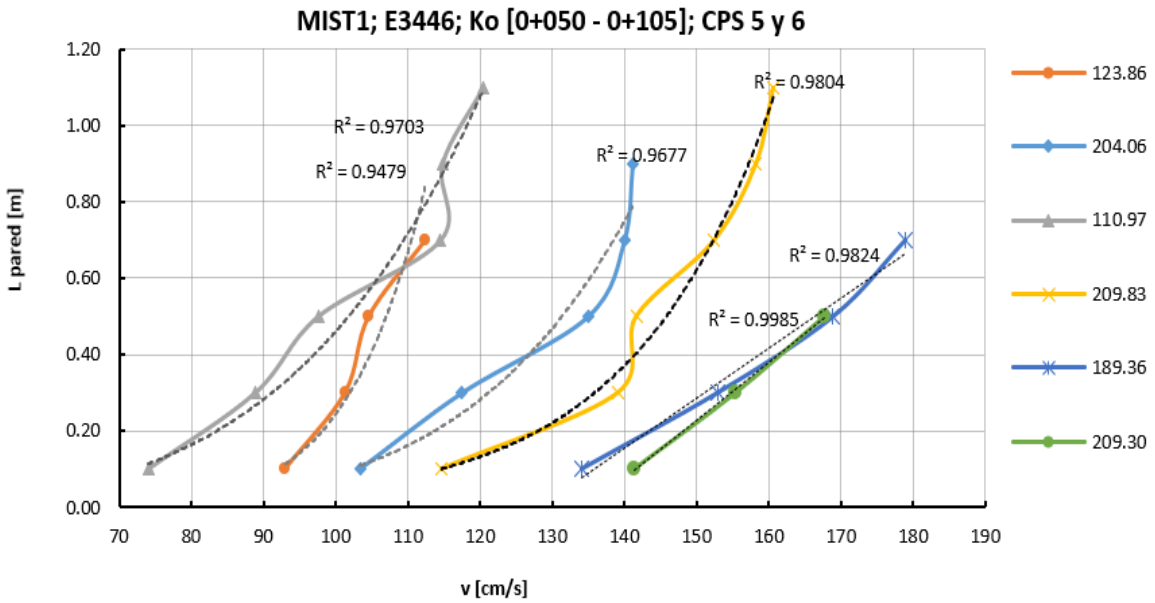

Figure 13. Velocity profiles were recorded by Doppler for different values of flow, from the Doppler located in Upper Left Bank Tunnel 1 (MIST1 K0+050).

Tecnología y ciencias del agua, ISSN 2007-2422, 13(2), DOI: 10.24850/j-tyca-2022-02-04

Open Access bajo la licencia CC BY-NC-SA 4.0 (https://creativecommons.org/licenses/by-nc-sa/4.0/)

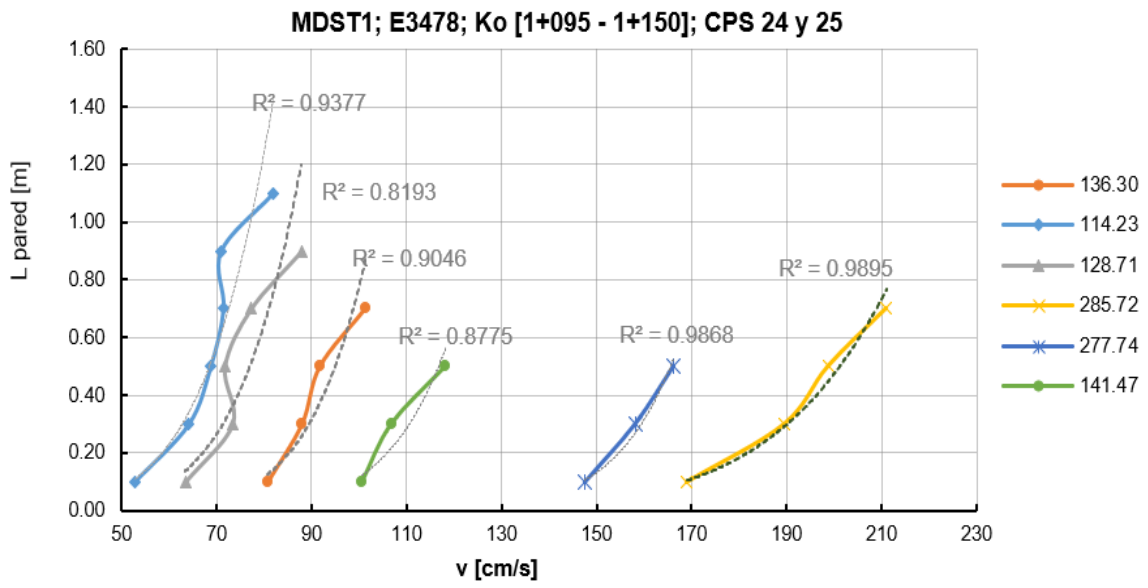

Figure 14. Velocity profiles were recorded by Doppler for different values of flow, from the Doppler located in the Upper Right Bank Tunnel 1 (MDST1 K1+095).

Open Access bajo la licencia CC BY-NC-SA 4.0 (https://creativecommons.org/licenses/by-nc-sa/4.0/)

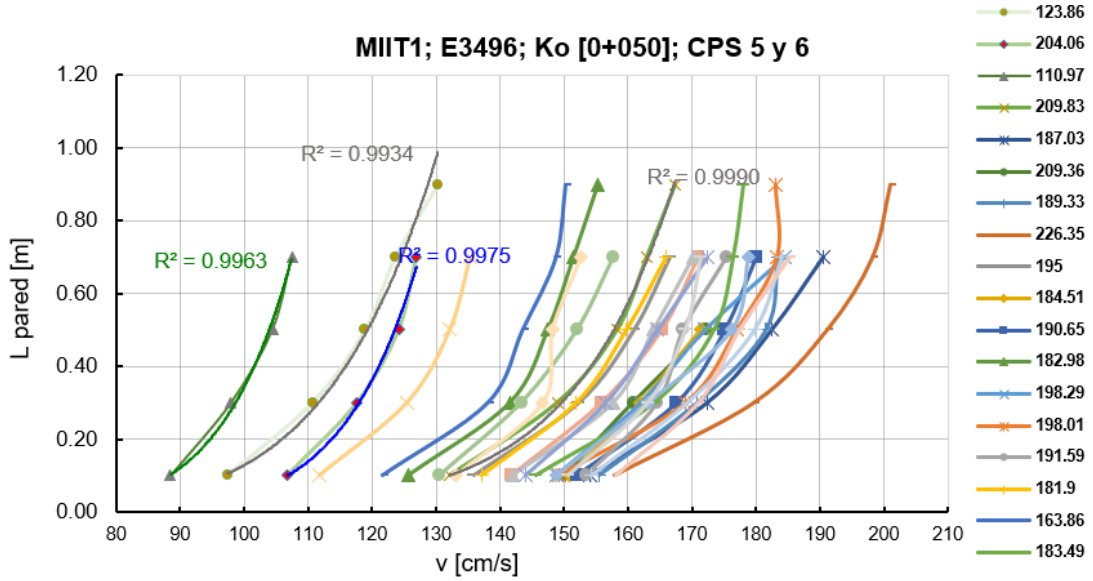

Figure 15. Velocity profiles were recorded by doppler for different values of flow, from the doppler located in Lower Left Bank Tunnel 1 (MIIT1 K1+050).

Estimates were made for different sections, and it was observed that the displacement thickness (δd) was about 10 % of the height water level value measured (Figure 16).

Tecnología y ciencias del agua, ISSN 2007-2422, 13(2), DOI: 10.24850/j-tyca-2022-02-04

Open Access bajo la licencia CC BY-NC-SA 4.0 (https://creativecommons.org/licenses/by-nc-sa/4.0/)

INFORMACIÓN PROVENIENTE DE ARGONAUTS EN TÚNEL 1 Y DE CELD

* revisados con la Ley Logarítmica

Vbeam	0.533	m
Press	0.099	dbar
1 Vbeam =	1.85741	bar
1 bar =	10.2	mca

			Ubicación						
		No.	1	2	3	4	y		nc
		Serie	MII T1	MIS T1	MDI T1	MDS T1	0+050	0+105	
			E3496	E3446	E3449	E3488	CPS-5	CPS-6	
Archivo	Celda	Q	I						
	Fecha/hr	m^3/s	h=2.5	h=5.5	h=4.0	h=7.0	m	m	Tramo 0+050 y
	OCTUBRE 09:00 (2011)								
MII009.ARG	05/10/2011 09:06	136.30	-	-	-	-	-	-	-
MIS006.ARG		136.30	-	-	-	-	-	-	-
MDI006.arg		136.30	-	-	-	-	-	-	-
MDS006.arg		136.30	-	-	-	-	-	-	-
MDS006.arg	13/10/2011 09:00	114.23	-	-	-	-	-	-	-
MDS006.arg	18/10/2011 09:00	128.71	-	-	-	-	-	-	-
MDS007.arg	27/10/2011 09:00	285.72	-	-	-	-	-	-	-
MDS007.arg	31/10/2011 09:09	277.74	-	-	-	-	-	-	-
	NOVIEMBRE 09:00 (2011)								
MDS007.arg	02/11/2011 09:15	141.47	-	-	-	-	-	-	-
	DICIEMBRE 09:00 (2011)								
1MII0002.arg	15/12/2011 09:00	123.86	OK	-	-	-	9.557	9.552	0.02657
1MIS0003.arg		123.86	-	OK	-	-	9.557	9.552	0.02657
MDI0002.arg		123.86	-	-	OK	-	9.557	9.552	0.02657
1MDS0003.arg		123.86	-	-	-	OK	9.557	9.552	0.02657
1MII0006.arg	20/12/2011 09:00	204.06	OK	-	-	-	9.209	9.198	0.02159
1MIS0003.arg		204.06	-	OK	-	-	9.209	9.198	0.02159
1MDI0004.arg		204.06	-	-	OK	-	9.209	9.198	0.02159
1MDS0005.arg		204.06	-	-	-	OK	9.209	9.198	0.02159
1MII0006.arg	23/12/2011 09:00	110.97	OK	-	-		9.211	9.210	0.01267
1MIS0003.arg		110.97	-	OK	-	-	9.211	9.210	0.01267
1MDI0004.arg		110.97	-	-	OK	-	9.211	9.210	0.01267
1MDS0005.arg		110.97	-	-	-	OK	9.211	9.210	0.01267
	ENERO 09:00 (2012)								
	FEBRERO 09:00 (2012)								
1MII0001.arg	18/02/2012 09:00	209.83	OK	-	-	-	9.756	9.773	0.02917
1MIS0001.arg		209.83	-	OK	-	-	9.756	9.773	0.02917
1MDI0001.arg		209.83	-	-	OK	-	9.756	9.773	0.02917
1MDS0001.arg		209.83	-	-	-	OK	9.756	9.773	0.02917

Archivo	Fecha/hr	1	2	3	4	5	6	7	8	9	10	δd
		Multi- Cell Data, Speed (cm/s)										
	OCTUBRE 09:00 (2011)	0.1	0.3	0.5	0.7	0.9	1.1	1.3	1.5	1.7	1.9	
MII009.ARG	05/10/2011 09:06	58.25	67.25	78.42	94.31	100.63	107.40	114.32	117.06	118.45	129.82	0.807
MIS006.ARG		78.03	96.73	97.52	103.49	113.10	121.54	116.22	126.92	131.75	130.22	1.030
MDI006.arg		93.67	104.38	110.76	118.76	131.63	130.19	128.13	132.75	130.32	129.04	0.665
MDS006.arg		80.71	87.91	91.71	101.34	107.50	107.47	113.95	122.93	125.68	122.58	0.558
MDS006.arg	13/10/2011 09:00	52.71	64.10	68.72	71.40	70.90	81.85	94.24	90.47	102.28	98.95	0.971
MDS006.arg	18/10/2011 09:00	63.45	73.31	71.70	77.20	87.81	92.52	98.13	102.99	100.23	107.20	0.879
MDS007.arg	27/10/2011 09:00	169.05	189.54	198.79	211.02	219.90	229.86	244.03	249.09	253.98	256.26	0.688
MDS007.arg	31/10/2011 09:09	147.41	158.10	166.31	175.33	192.01	186.49	205.79	212.31	213.15	225.35	0.492
	NOVIEMBRE 09:00 (2011)											
MDS007.arg	02/11/2011 09:15	100.63	106.80	118.22	123.21	123.53	133.18	130.7	134.25	135.3	140.07	0.417
	DICIEMBRE 09:00 (2011)											
1MII0002.arg	15/12/2011 09:00	97.46	110.69	118.91	123.62	130.29	132.58	131.01	131.31	129.7	128.47	0.755
1MIS0003.arg		93.04	101.32	104.58	112.37	123.65	131.2	120.84	126.23	125.22	122.05	0.565
MDI0002.arg		73.51	79.00	82.14	84.71	84.02	83.53	83.1	87.7	83.1	89.51	0.496
1MDS0003.arg		65.09	70.19	82.93	87.06	86.3	82.9	85.24	84.05	91.22	83.74	0.514
1MII0006.arg	20/12/2011 09:00	106.78	117.68	124.19	126.93	131.94	132.94	133.08	130.49	130.75	126.54	0.602
1MIS0003.arg		103.34	117.52	134.96	139.96	141.09	141.89	145.23	152.72	154.61	150.01	0.735
1MDI0004.arg		80.42	91.39	97.43	97.65	102.52	98.3	95.9	88.93	93.8	101.2	0.732
1MDS0005.arg		79.88	97.71	111.75	107.25	111.3	112.5	120.31	119.37	116.88	118.45	0.974
1MII0006.arg	23/12/2011 09:00	88.48	97.95	104.42	107.45	110	106.81	108.87	111.5	110.34	106.59	0.623
1MIS0003.arg		74.10	88.90	97.61	114.54	114.77	120.39	119.36	114.51	114.89	120.66	0.918
1MDI0004.arg		73.72	85.00	75.34	75.62	71	69.9	72.36	71.3	65.4	67.53	0.787
1MDS0005.arg		61.63	74.16	80.99	82.8	83.6	81.7	82.8	84.71	80.56	84.92	0.927
	ENERO 09:00 (2012)	74.10	88.90	97.61	114.54	114.77	120.39	119.36	114.51	114.89	120.66	
	FEBRERO 09:00 (2012)											
1MII0001.arg	18/02/2012 09:00	132.21	148.96	158.29	162.9	167.37	165.27	169.15	166.72	165.62	163.86	0.737
1MIS0001.arg		114.68	139.11	141.66	152.46	158.24	160.64	164.49	166.18	164.41	167.47	1.002
1MDI0001.arg		116.93	122.85	129.06	124.01	131.85	126.2	128.1	124.3	128.12	126.98	0.372
1MDS0001.arg		113.51	125.20	132.46	138.03	137.1	146.31	142.42	142.45	143.02	147.13	0.640

Figure 16. Review of the displacement thickness δd.

Applying Equation (22) and the methodology described in the "Nikuradse equivalent roughness *ks* " subchapter, n_{pared} wall roughness values were obtained (Table 4, Figure 17, Figure 18, Figure 19, and Figure 20). For Doppler equipment located at sections K0+050 and K1+115 of Tunnel 1 and located at different heights: Lower Left Margin Tunnel 1 (MII T1) in *h* = 2. 5 m; Tunnel 1 Upper Left Bank (MIS T1) in *h* = 5.5 m; Tunnel 1 Lower Right Bank (MDI T1) in *h* = 4 m; Tunnel 1 Upper Right Bank (MDS T1) in *h* = 7 m.

Open Access bajo la licencia CC BY-NC-SA 4.0 (https://creativecommons.org/licenses/by-nc-sa/4.0/)

Table 4. Wall roughness values (n_{pared}) in shotcrete for doppler at K0+050 and K1+115.

Section 0+050		n_{pared}	***h* (m)**
MII T1	E3496	0.0121	2.5
MIS T1	E3446	0.0154	5.5
MDI T1	E3449	0.0104	4
MDS T1	E3488	0.0193	7

Section 1+115		n_{pared}	***h* (m)**
MII T1	E3465	0.0278	2.5
MIS T1	E3497	0.0174	5.5
MDI T1	E3479	0.0139	4
MDS T1	E3478	0.0134	7

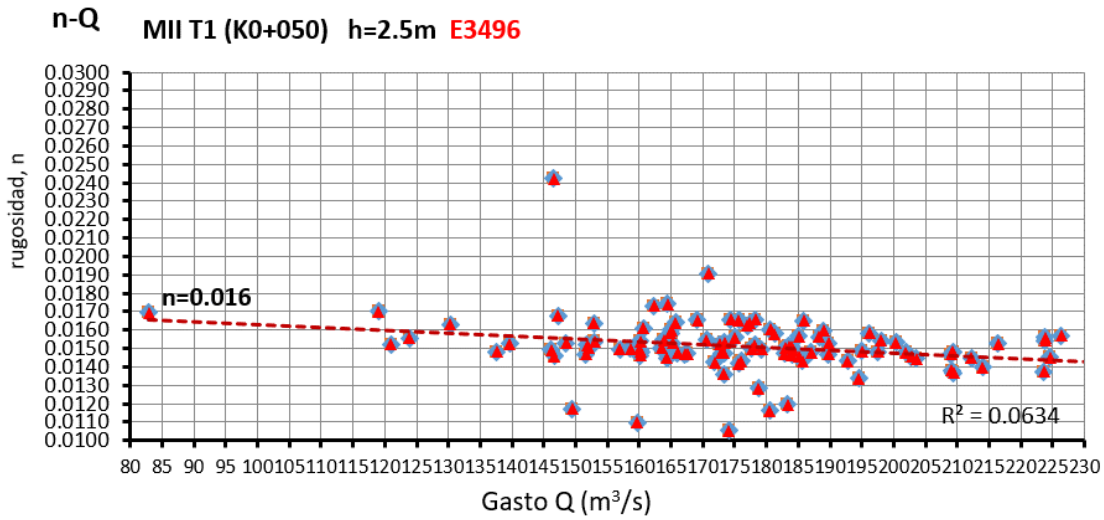

Figure 17. Roughness-flow graph for Doppler at 2.5 m (MII T1 at K0+050). Representative roughness n = 0.016.

Tecnología y ciencias del agua, ISSN 2007-2422, 13(2), DOI: 10.24850/j-tyca-2022-02-04

Open Access bajo la licencia CC BY-NC-SA 4.0 (https://creativecommons.org/licenses/by-nc-sa/4.0/)

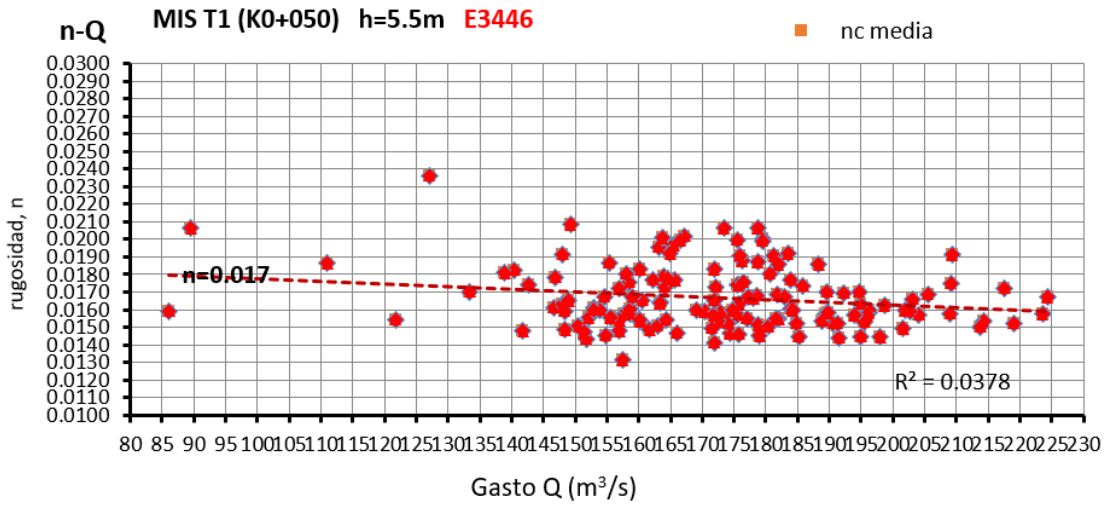

Figure 18. Roughness-flow graph for Doppler located at 5.5 m (MIS T1 at K0+050). Representative roughness *n* = 0.017.

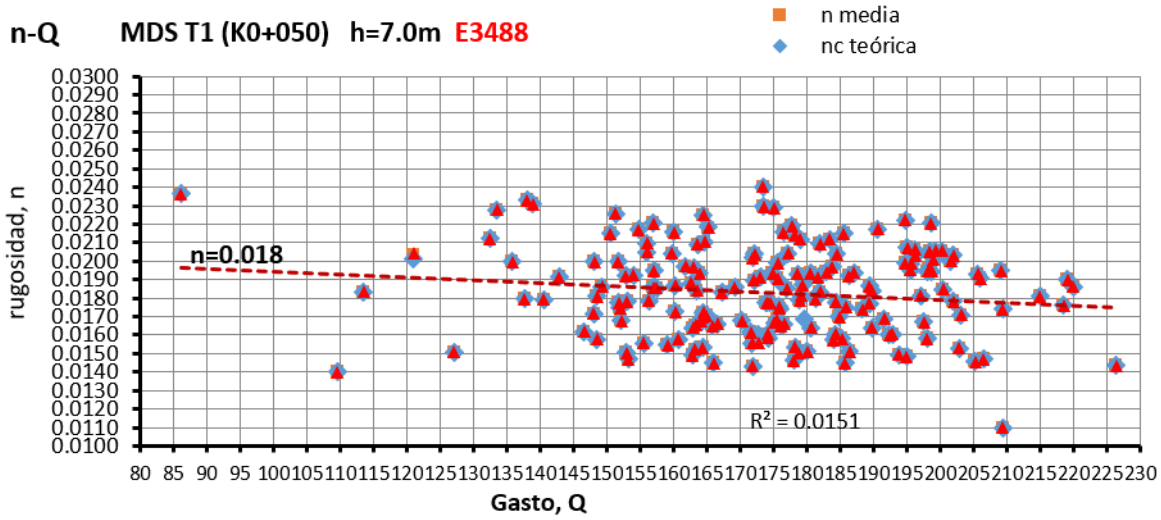

Figure 19. Roughness - flow graph for Doppler located at 7 m (MDS T1 at K0+050). Representative roughness *n* = 0.018.

Open Access bajo la licencia CC BY-NC-SA 4.0 (https://creativecommons.org/licenses/by-nc-sa/4.0/)

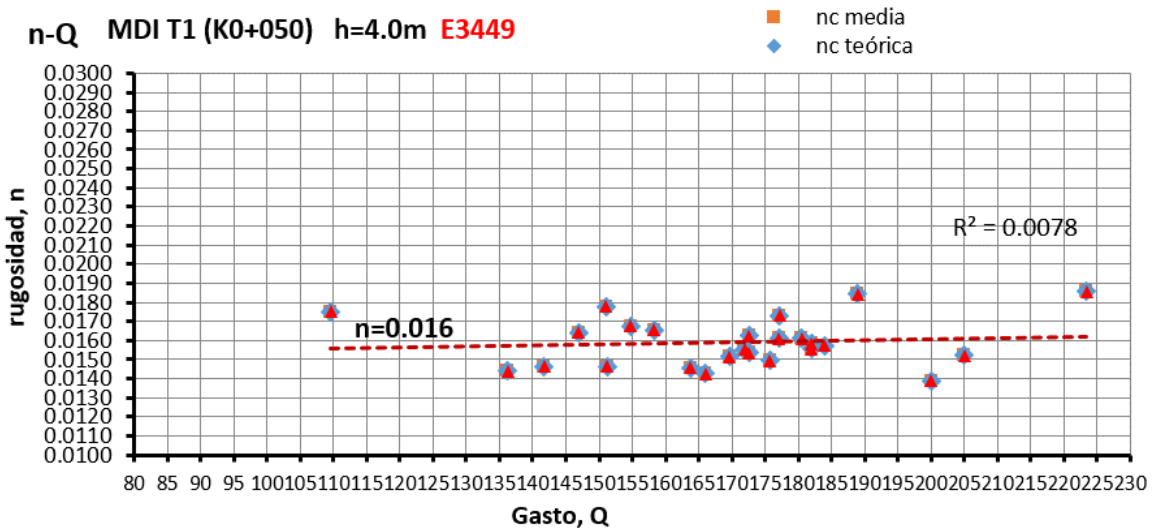

Figure 20. Roughness - flow graph for Doppler located at 4 m (MDI T1 at K0+050). Representative roughness *n* = 0.016.

As for water level height, it was observed that the roughness does not change significantly, as is the case with the flow, even when it is increased by 30 cm. The representative roughness is in the range of *n* = 0.019 (Figure 21, Figure 22, and Figure 23).

Tecnología y ciencias del agua, ISSN 2007-2422, 13(2), DOI: 10.24850/j-tyca-2022-02-04

Open Access bajo la licencia CC BY-NC-SA 4.0
(https://creativecommons.org/licenses/by-nc-sa/4.0/)

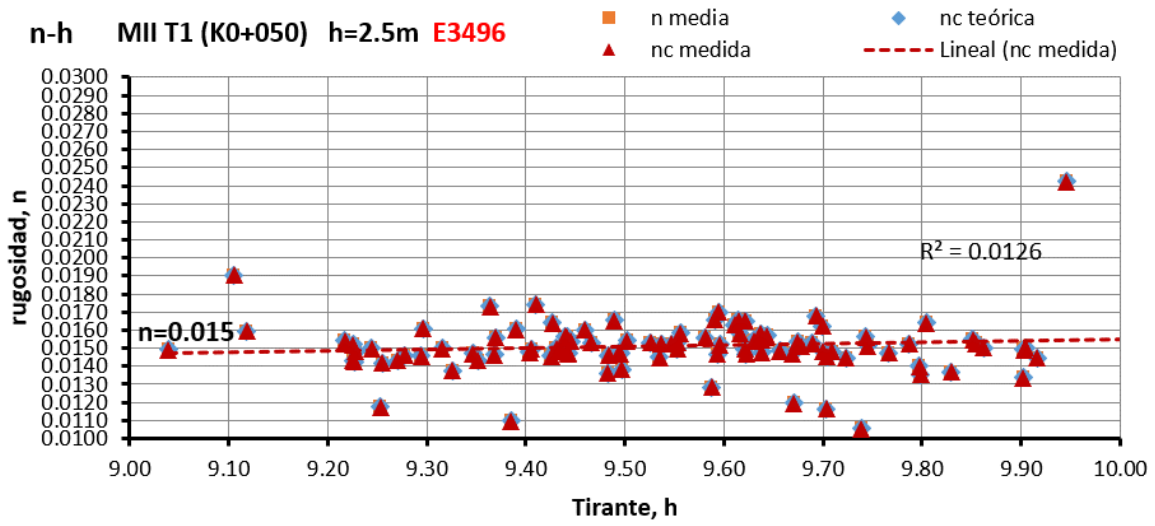

Figure 21. The roughness-level graph was obtained from the doppler at 2.5 m (MII T1 at K0+050). Representative roughness *n* = 0.015.

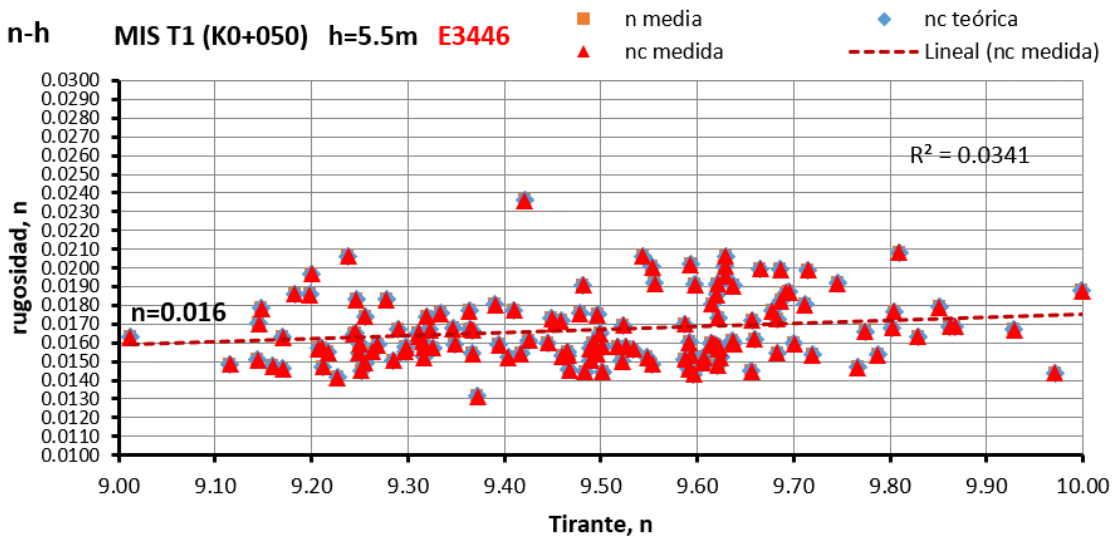

Figure 22. The roughness-level graph was obtained from the doppler at 5.5 m (MIS T1 at K0+050). Representative roughness *n* = 0.016.

Tecnología y ciencias del agua, ISSN 2007-2422, 13(2), DOI: 10.24850/j-tyca-2022-02-04

Open Access bajo la licencia CC BY-NC-SA 4.0 (https://creativecommons.org/licenses/by-nc-sa/4.0/)

S EN TÚNEL 1 Y DE CELDAS DE MARZO DE 2012 A OCTUBR

Estimación del Parámetro ks, a partir de la aplicación directa de :

"Ley Logarítmica de Distribución de velocidades"

$$\beta = \upsilon_2 - \left(\frac{\upsilon_2 - \upsilon_1}{\eta_2 - \eta_1}\right)\eta_2 \qquad k_{s,ch,cl} = g^3\left(\frac{n_{ch,cl}}{K_m}\right)^6$$

$$ks = e^{\left(kB - \frac{\beta}{\upsilon_*}\right)} \qquad \text{Donde: } \upsilon_* = \alpha = \frac{\upsilon_2 - \upsilon_1}{\eta_2 - \eta_1} \qquad f = 8k_m^{\,2}(ks/Rh)^{1/3}$$

Metodologia de cálculo de la Rugosidad puntual mediante Argonauts

Celda	Q	Ubicación 1	2	3	4	y		nc	velocidad (m/s		Long, con respecto a la		$\eta=\ln\alpha^*=\ln y$		ctes.			β	v*	ks	f	n_{pa}	COEF. CORR	R2
		MII T1	MIS T1	MDI T1	MDS T1	0+050	0+105																	
		E3496	E3446	E3449	E3488	CPS-5	CPS-6																	
Fecha/hr	m^3/s	h=2.5	h=5.5	h=4.0	h=7.0	m	m	Tramo 0+050 y	υ_1	υ_2	ζ_1	ζ_2	η_1	η_2	k	B	km							
05/10/2011 09:06	136.30	-	-	-	-	-	-	-	0.58	0.67	0.1	0.3	-2.3	-1.2	0.4	8.5	0.13	0.77	0.082	0.0024	0.0113	0.015	0.9915	0.9832
	136.30	-	-	-	-	-	-	-	0.78	0.97	0.1	0.3	-2.3	-1.2	0.4	8.5	0.13	1.17	0.17	0.0306	0.0262	0.023	0.9476	0.8980
	136.30	-	-	-	-	-	-	-	0.94	1.04	0.1	0.3	-2.3	-1.2	0.4	8.5	0.13	1.16	0.097	0.0002	0.0049	0.010	0.9946	0.9893
	136.30	-	-	-	-	-	-	-	0.81	0.88	0.1	0.3	-2.3	-1.2	0.4	8.5	0.13	0.96	0.066	0.0000	0.0020	0.006	0.9844	0.9691
13/10/2011 09:00	114.23	-	-	-	-	-	-	-	0.53	0.64	0.1	0.3	-2.3	-1.2	0.4	8.5	0.13	0.77	0.104	0.0186	0.0222	0.021	0.8919	0.7954
18/10/2011 09:00	128.71	-	-	-	-	-	-	-	0.63	0.73	0.1	0.3	-2.3	-1.2	0.4	8.5	0.13	0.84	0.09	0.0025	0.0114	0.015	0.8838	0.7811
27/10/2011 09:00	285.72	-	-	-	-	-	-	-	1.69	1.9	0.1	0.3	-2.3	-1.2	0.4	8.5	0.13	2.12	0.187	0.0003	0.0059	0.011	0.9770	0.9546
31/10/2011 09:09	277.74	-	-	-	-	-	-	-	1.47	1.58	0.1	0.3	-2.3	-1.2	0.4	8.5	0.13	1.7	0.097	0.0000	0.0008	0.004	1.0000	1.0000
02/11/2011 09:15	141.47	-	-	-	-	-	-	-	1.01	1.07	0.1	0.3	-2.3	-1.2	0.4	8.5	0.13	1.14	0.056	0.0000	0.0003	0.003	1.0000	1.0000
15/12/2011 09:00	123.86	OK	-	-	-	9.557	9.552	0.02657	0.97	1.11	0.1	0.3	-2.3	-1.2	0.4	8.5	0.13	1.25	0.12	0.0009	0.0081	0.013	0.9766	0.9537
	123.86	-	OK	-	-	9.557	9.552	0.02657	0.93	1.01	0.1	0.3	-2.3	-1.2	0.4	8.5	0.13	1.1	0.075	0.0000	0.0020	0.006	0.9699	0.9407
	123.86	-	-	OK	-	9.557	9.552	0.02657	0.74	0.79	0.1	0.3	-2.3	-1.2	0.4	8.5	0.13	0.85	0.05	0.0000	0.0009	0.004	0.9879	0.9759
	123.86	-	-	-	OK	9.557	9.552	0.02657	0.65	0.7	0.1	0.3	-2.3	-1.2	0.4	8.5	0.13	0.76	0.046	0.0000	0.0011	0.005	0.9708	0.9424
20/12/2011 09:00	204.06	OK	-	-	-	9.209	9.198	0.02159	1.07	1.18	0.1	0.3	-2.3	-1.2	0.4	8.5	0.13	1.3	0.099	0.0001	0.0034	0.008	0.9896	0.9792
	204.06	-	OK	-	-	9.209	9.198	0.02159	1.03	1.18	0.1	0.3	-2.3	-1.2	0.4	8.5	0.13	1.33	0.129	0.0010	0.0084	0.013	0.9800	0.9604
	204.06	-	-	OK	-	9.209	9.198	0.02159	0.8	0.91	0.1	0.3	-2.3	-1.2	0.4	8.5	0.13	1.03	0.1	0.0010	0.0083	0.013	0.9231	0.8521
	204.06	-	-	-	OK	9.209	9.198	0.02159	0.8	0.98	0.1	0.3	-2.3	-1.2	0.4	8.5	0.13	1.17	0.162	0.0218	0.0235	0.022	0.8554	0.7318
23/12/2011 09:00	110.97	OK	-	-		9.211	9.210	0.01267	0.88	0.98	0.1	0.3	-2.3	-1.2	0.4	8.5	0.13	1.08	0.086	0.0001	0.0040	0.009	0.9941	0.9883
	110.97	-	OK	-	-	9.211	9.210	0.01267	0.74	0.89	0.1	0.3	-2.3	-1.2	0.4	8.5	0.13	1.05	0.135	0.0122	0.0194	0.020	0.9730	0.9466
	110.97	-	-	OK	-	9.211	9.210	0.01267	0.74	0.85	0.1	0.3	-2.3	-1.2	0.4	8.5	0.13	0.97	0.103	0.0023	0.0111	0.015	-0.0998	0.0100
	110.97	-	-	-	OK	9.211	9.210	0.01267	0.62	0.74	0.1	0.3	-2.3	-1.2	0.4	8.5	0.13	0.88	0.114	0.0135	0.0200	0.020	0.9061	0.8210
18/02/2012 09:00	209.83	OK	-	-	-	9.756	9.773	0.02917	1.32	1.49	0.1	0.3	-2.3	-1.2	0.4	8.5	0.13	1.67	0.152	0.0005	0.0067	0.012	0.9657	0.9325
	209.83	-	OK	-	-	9.756	9.773	0.02917	1.15	1.39	0.1	0.3	-2.3	-1.2	0.4	8.5	0.13	1.66	0.222	0.0173	0.0216	0.021	0.9472	0.8972

Figure 23. Calculation of the equivalent roughness *ks* and the parameters *f* and *n*.

Additionally, it was observed that the roughness varies slightly in the reinforced zones (K0+160 to K0+215 and from K0+380 to K0+435). These zones have smooth concrete since they are structurally reinforced zones (Figure 24).

Tecnología y ciencias del agua, ISSN 2007-2422, 13(2), DOI: 10.24850/j-tyca-2022-02-04

Open Access bajo la licencia CC BY-NC-SA 4.0 (https://creativecommons.org/licenses/by-nc-sa/4.0/)

	Sección	Celda	Cad.	Rugosidad
CASETA 1	1 2	CPS - 4 CPS - 5	0+007 0+050	Concreto Hidráulico Concreto Lanzado
	2 3	CPS - 5 CPS - 6	0+050 0+105	Concreto Lanzado Concreto Hidráulico
	3 4	CPS - 6 CPS - 7	0+105 0+160	Concreto Lanzado Concreto Hidráulico
	4 5	**CPS - 7 CPS - 8**	**0+160 0+215**	**Concreto Hidráulico (Casquillo)**
	5 6	CPS - 8 CPS - 9	0+215 0+270	Concreto Lanzado Concreto Hidráulico
	6 7	CPS - 9 CPS - 10	0+270 0+325	Concreto Lanzado
	7 8	CPS - 10 CPS - 11	0+325 0+380	Concreto Lanzado
	8 9	**CPS - 11 CPS - 12**	**0+380 0+435**	**Concreto Lanzado (Casquillo)**
	9 10	CPS - 12 CPS - 13	0+435 0+490	Concreto Lanzado Concreto Hidráulico
	10 11	CPS - 13 CPS - 14	0+490 0+545	Concreto Lanzado

Figure 24. Location of roughness zones (shotcrete and hydraulic concrete).

Two graphs are shown: one for flows greater than 150 m^3/s (Figure 25), and one for flows less than 150 m^3/s (Figure 26), where roughness changes are observed.

Open Access bajo la licencia CC BY-NC-SA 4.0 (https://creativecommons.org/licenses/by-nc-sa/4.0/)

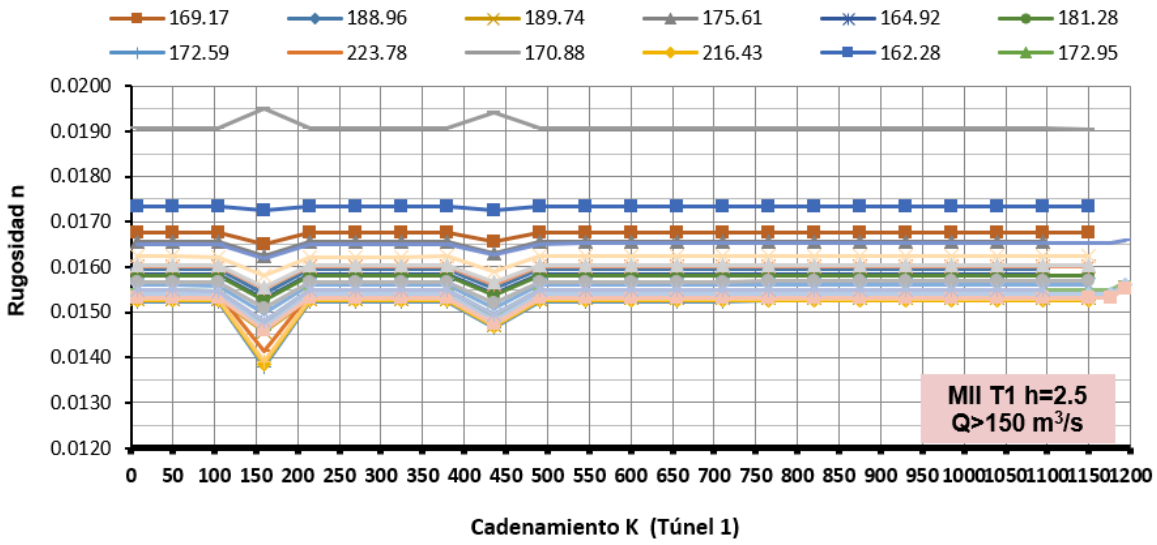

Figure 25. Composite roughness along the tunnel for a Q > 150 m^3/s. Doppler at 2.5 m height.

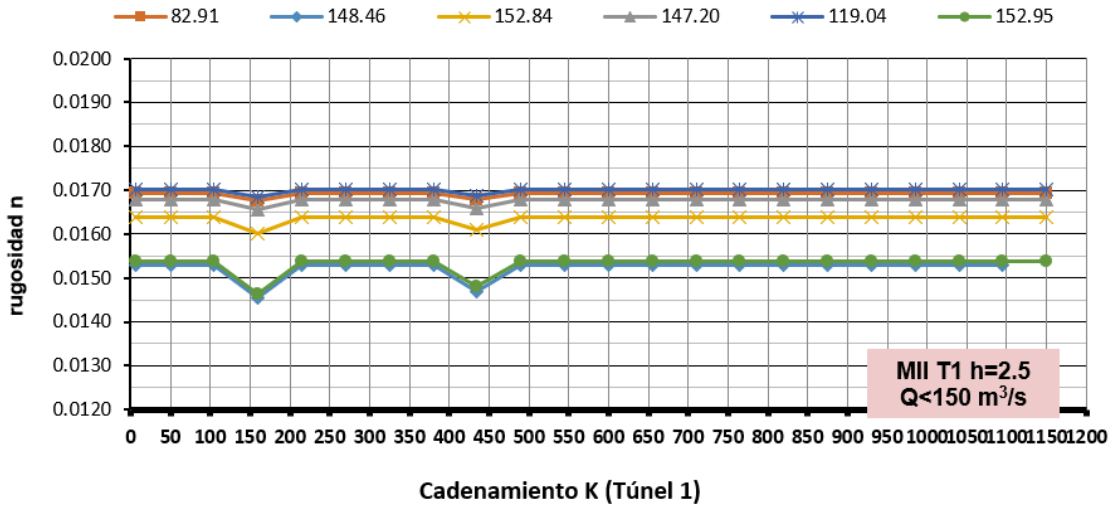

Figure 26. Composite roughness along the tunnel for a Q < 150 m^3/s. Doppler at 2.5 m height.

Tecnología y ciencias del agua, ISSN 2007-2422, 13(2), DOI: 10.24850/j-tyca-2022-02-04

Open Access bajo la licencia CC BY-NC-SA 4.0 (https://creativecommons.org/licenses/by-nc-sa/4.0/)

Figure 27 also shows that the flow among sections remains very similar between the first and the last sensor (section) for the values taken every hour so that the calculation can be taken as a permanent flow.

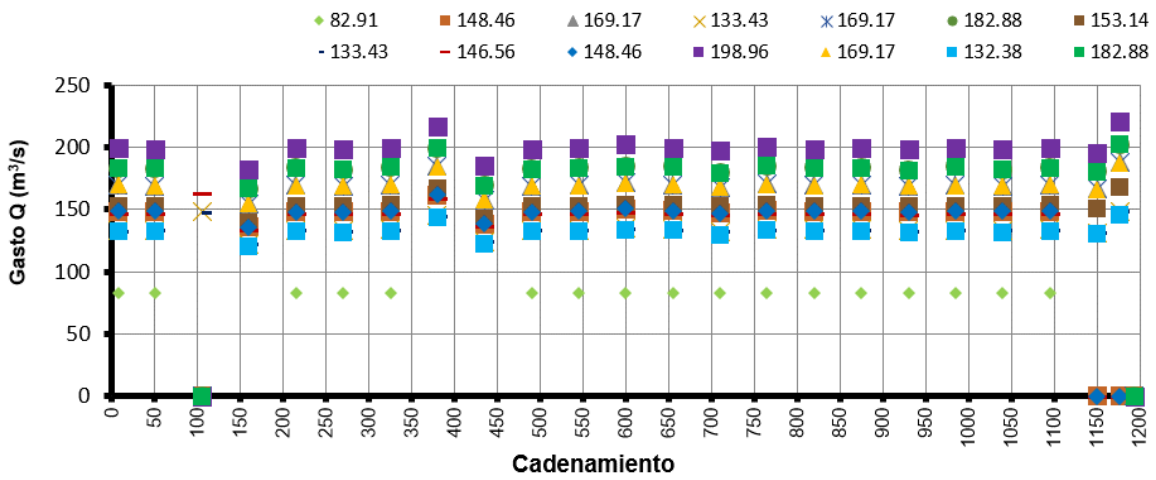

Figure 27. Flow along the tunnel (per sensor).

The following graphs (Figure 28, Figure 29, Figure 30, and Figure 31) show the hydraulic profile of some of the modeled and calibrated outflows, the blue line represents the theoretical value, and the black dots the measured values.

Tecnología y ciencias del agua, ISSN 2007-2422, 13(2), DOI: 10.24850/j-tyca-2022-02-04

Open Access bajo la licencia CC BY-NC-SA 4.0 (https://creativecommons.org/licenses/by-nc-sa/4.0/)

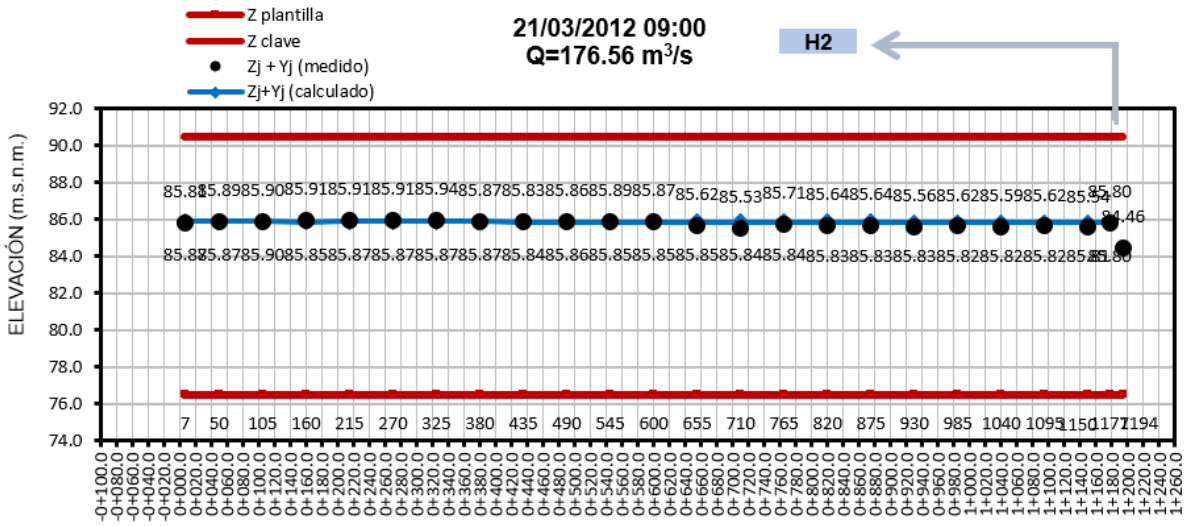

Figure 28. Model calibration for Q = 176.56 m^3/s.

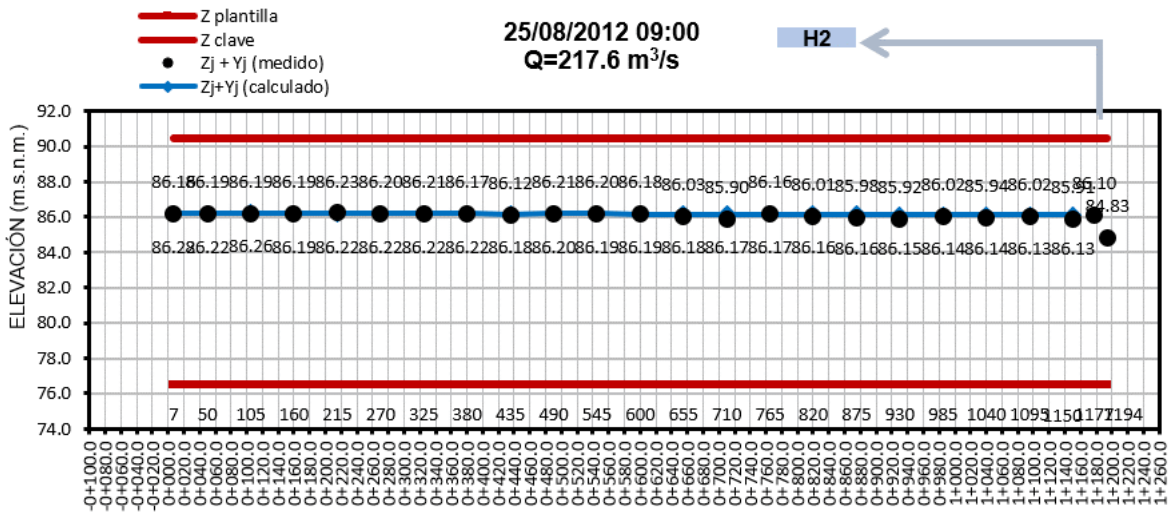

Figura 29. Model calibration for Q = 217.6 m^3/s.

Open Access bajo la licencia CC BY-NC-SA 4.0 (https://creativecommons.org/licenses/by-nc-sa/4.0/)

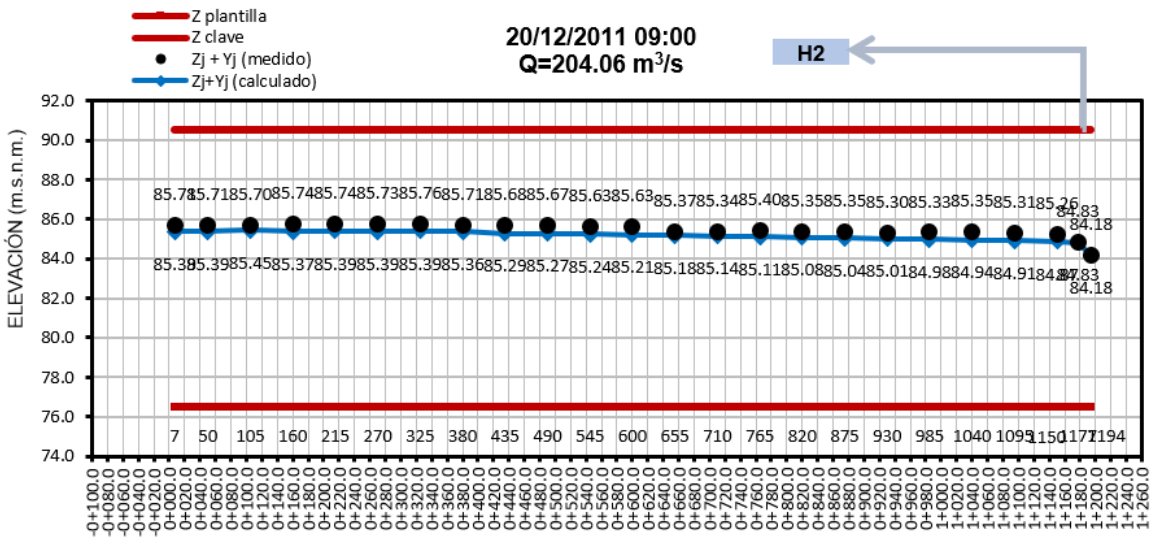

Figure 30. Model calibration for Q = 204.06 m^3/s.

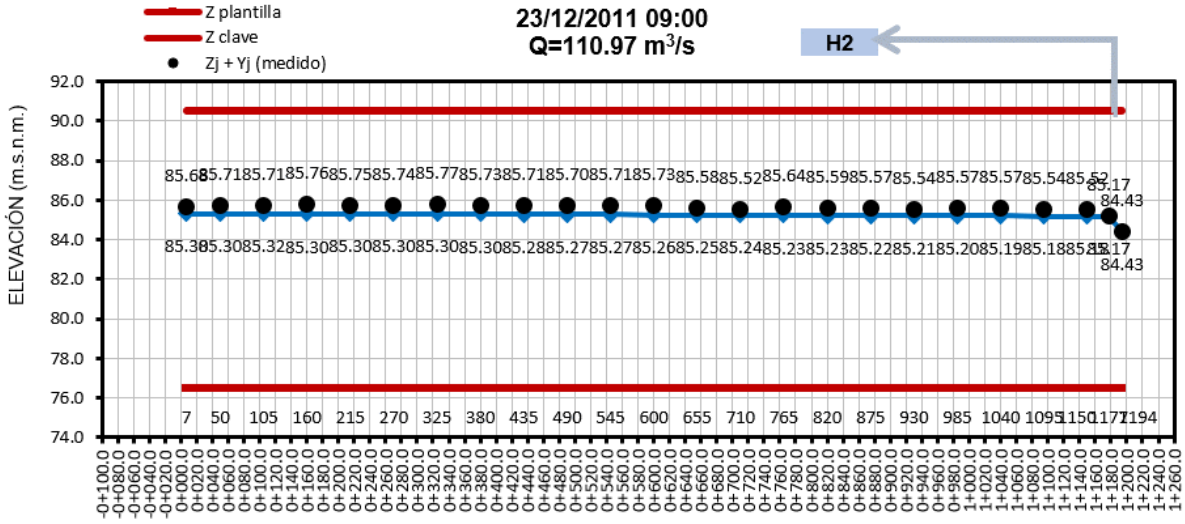

Figure 31. Model calibration for Q = 110.97 m^3/s.

Open Access bajo la licencia CC BY-NC-SA 4.0 (https://creativecommons.org/licenses/by-nc-sa/4.0/)

Each of the three calibrated composite roughness values was reviewed: $n_{c\text{-}EHG}$, Equation (12); $n_{c\text{-}measured}$, Equation (22); $n_{c\text{-}theoretical}$ (Equations Table 3), and minimum squared error was identified for all sections with level sensors. Those with the lowest standard deviation value were discretized and identified.

In the sections along the tunnel, different roughness values were identified, after discretizing and calibrating them regarding the measurements and the calculation described before with the general hydraulic equation, the following values were found with the minimum square error (MSE), which are equivalent to an average composite roughness for Tunnel 1 of **0.0178** (Figure 32).

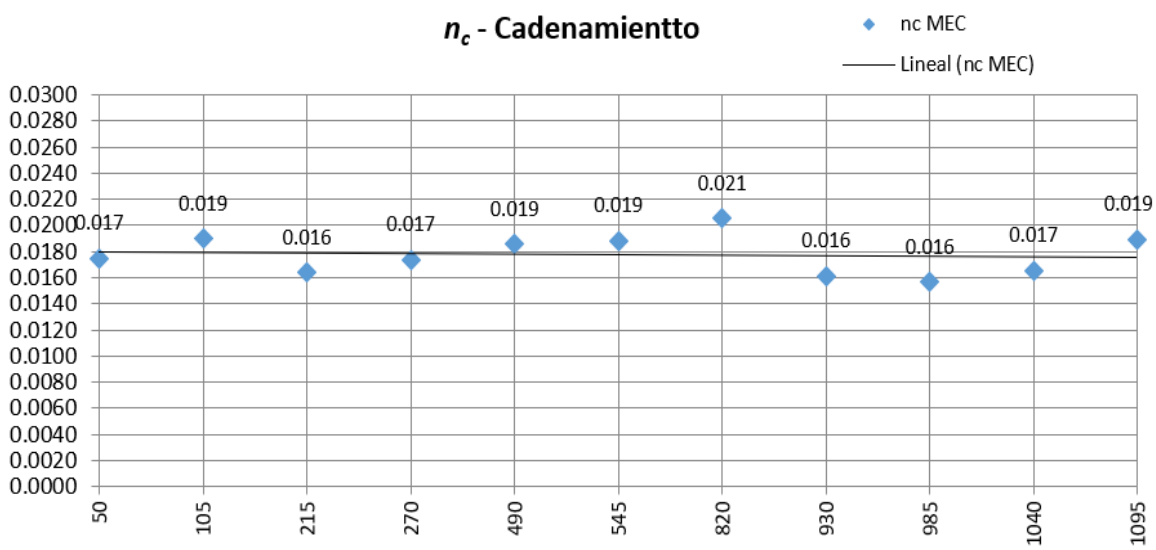

Figure 32. Composite roughness with MSE, per section.

Tecnología y ciencias del agua, ISSN 2007-2422, 13(2), DOI: 10.24850/j-tyca-2022-02-04

Open Access bajo la licencia CC BY-NC-SA 4.0 (https://creativecommons.org/licenses/by-nc-sa/4.0/)

Figure 33 shows the trend of the composite roughness values obtained for a range of flow rates from 130 to 210 m^3/s, which were discretized and calibrated from the theoretical model and the methodology proposed for the 17 equations, as well as the measurements.

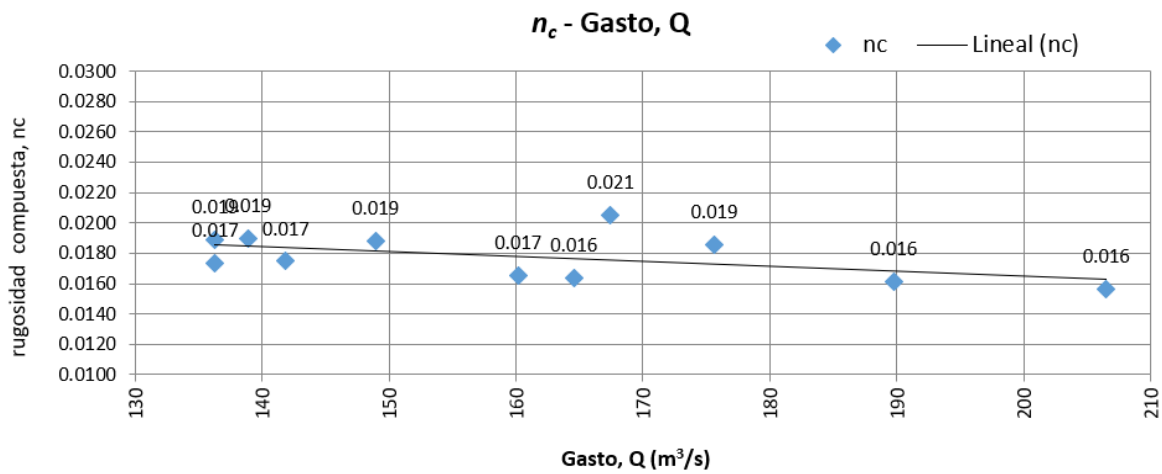

Figure 33. Composite roughness (n_c) concerning measured flow (Q).

The equation with the best adjustment of the 17 known equations (Table 3) was identified with the letter "I", for a range of flows ranging from 85 to 285 m^3/s:

Equation I (15) (Chie-Yen, 2002):

Tecnología y ciencias del agua, ISSN 2007-2422, 13(2), DOI: 10.24850/j-tyca-2022-02-04

Open Access bajo la licencia CC BY-NC-SA 4.0 (https://creativecommons.org/licenses/by-nc-sa/4.0/)

$$I = n_c = \left[\frac{R^{1/3}}{P}\sum\frac{n_i^2 P_i}{R_i^{1/3}}\right]^{1/2} \tag{25}$$

Figure 34 shows the best adjustment composite roughness equations n_c for each flow.

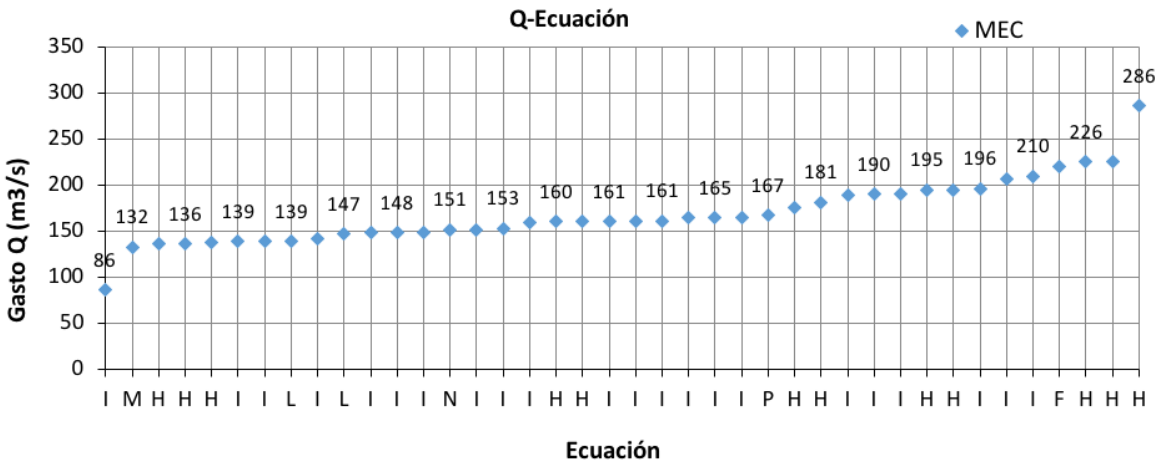

Figure 34. Equations of best adjustment for each calibrated flow.

Likewise, it was possible to identify that the integration of the mentioned methodologies allows for a better definition of the composite roughness parameter in addition to the empirical equations Chie-Yen, 2002). Then through hydraulic instrumentation, velocities can be measured in the areas close to the wall and, complemented with water height level (sensors) and flow measurements, the equivalent roughness parameter can be had by integrating the Logarithmic Law of velocities and

Tecnología y ciencias del agua, ISSN 2007-2422, 13(2), DOI: 10.24850/j-tyca-2022-02-04

Open Access bajo la licencia CC BY-NC-SA 4.0 (https://creativecommons.org/licenses/by-nc-sa/4.0/)

the Nikuradse and Prandtl-Von Kármán equations, arriving finally at the representative composite roughness of the section or tunnel. This methodology can be applied to wide channels hydraulically rough and in permanent regime conditions where it is possible to integrate the Darcy-Weisbach and Manning relationship (Aldama & Ocón, 2012).

Previous experimental studies have been carried out to determine the composite roughness in tunnels using prototype models (Marengo & Arreguín, 2008). In 2007 an experimental investigation was carried out, where the flow was compared with four tunnel models in an arch section working as a channel, with different roughnesses, and under different runoff conditions. The prototype studied four associated roughnesses: acrylic, sandpaper, and plastic, which resemble hydraulic concrete, shotcrete, and prototype rock. The following approximations were obtained from the experimental results: 1) for the Acrylic-Sandpaper combination, the best approximation was obtained with the Ida-Engelund M Equation; 2) for the Acrylic-Plastic combination, the best-fit equation was Felkel's F; 3) finally, the author recommended that due to the turbulence that occurs in reality, the Felkel Equations (Equation F), Yen's Equation (Equation H) and Yen's Equation N should also be used (see Table 3).

Conclusions

Tecnología y ciencias del agua, ISSN 2007-2422, 13(2), DOI: 10.24850/j-tyca-2022-02-04

Open Access bajo la licencia CC BY-NC-SA 4.0 (https://creativecommons.org/licenses/by-nc-sa/4.0/)

The approach of the developed methodology allows for the studying of the composite roughness through the relationship between the contact surface and the fluid (boundary layer zone), applying the Prandtl-Von Kármán boundary layer theories using the velocity profiles obtained from hydraulic instrumentation using measurements very close to the wall. This was applied to the case study of Tunnel 1 of the Grijalva River. The results were obtained from the Nikuradse equivalent roughness *ks*, and with the relationship between the Darcy-Weisbach and Manning equations, a wall roughness was obtained. Aside from this, with a general hydraulic model and section measurements, a representative tunnel roughness of n = 0.0178 was obtained. It was observed that along the tunnel, the roughness value remains constant except for places where the surface is changed to smooth concrete. It was also found that Yen's Equation I (Chie-Yen, 2002) is the best approximation. Even though the composite roughness did not have a significant variation in the range of the analyzed flow rates (117 to 575 m^3/s), it is recommended to continue with the measurement and to apply the methodology for higher flows since variations in roughness could only be observed if flow increases significantly. It is also recommended to continue with the water levels, flow, and velocity records to carry out the calibration with measured data.

Implementing hydraulic instrumentation in real conditions in tunnels and channels is an important research tool for the study of composite

Open Access bajo la licencia CC BY-NC-SA 4.0 (https://creativecommons.org/licenses/by-nc-sa/4.0/)

roughness in the design of these structures, which improves existing empirical methods. Previous studies on these topics have been carried out on prototype models, however, this study additionally integrates a scale deviation parameter.

The use of composite roughness, i.e., combined roughness of smooth concrete and shotcrete in tunnels, ensures more efficient hydraulic performance in tunnels of dams, guaranteeing a better hydraulic discharge capacity in a contingency event during dam construction since it allows the integration of a longer return period (Tr). It also maintains a better cost/benefit ratio by not obligating a complete recoat of all the sections with hydraulic concrete.

According to Marengo (2019), in recent years great importance has been given to durability and failure conditions in dams and their temporary structures such as channels and tunnels. It is necessary to review these events from the technical, social and legal points of view. Additionally, the development of numerical methods and computational techniques allow for arriving at better knowledge and understanding of hydrological, geological, and materials aspects, among others. It is also necessary to implement instrumentation projects for defining the hydraulic and structural behavior of dams.

The consideration of the evaluation of the failure risks together with the composite roughness analysis methods applied in this research would allow for better elements for designing new projects.

Acknowledgments

Open Access bajo la licencia CC BY-NC-SA 4.0 (https://creativecommons.org/licenses/by-nc-sa/4.0/)

To the Hydraulics Laboratory of the Federal Electricity Commission and the colleagues in the laboratory and field. To the Coordination of Hydropower Projects of the CFE for the opportunity to collaborate directing several projects and studies of instrumentation in hydraulic structures. To Dr. Humberto Marengo who was the Coordinator of Hydropower Projects and promoter of these topics. And to Dr. Alvaro Aldama who advised this and several projects on the fundamental concepts of Fluid Mechanics that opened the way for this research.

References

Aldama, A. A., & Ocón, A. R. (enero-marzo, 2002). Resistencia al flujo en canales y límites de aplicabilidad de la fórmula Manning. *Ingeniería Hidráulica en México*, 17(1), 107-115.

Chie-Yen, B. F. (January 2002). Open Channel Flow Resistance. *Journal of Hydraulic Engineering*, 128(1). DOI: 10.1061/(ASCE)0733-9429(2002)128:1(20).

Chow, V. T. (1959). *Hidráulica de canales abiertos*. Tokyo, Japón: McGraw Hill. Kogakusha, LTD.

Marengo, H. (2019). *Obras de desvío en proyectos hidráulicos, aspectos de diseño y construcción*. Ciudad de México, México: Instituto de Ingeniería, Universidad Nacional Autónoma de México.

Marengo, H. (2011). *Deslizamiento de tierra y roca que obstruyó el río Grijalva y su solución con túneles*. Conferencia CFE. Tercer Seminario de Potamología. IMTA, Jiutepec, Morelos, México.

Open Access bajo la licencia CC BY-NC-SA 4.0 (https://creativecommons.org/licenses/by-nc-sa/4.0/)

Marengo, H., & Arreguín, F. (enero-marzo, 2008). Análisis hidráulico experimental en túneles de conducción en sección baúl trabajando como canal, considerando rugosidades compuestas. *Ingeniería Hidráulica en México*, 23(1), 21-44.

Rouse, H. (1965). Critical analysis of open channel resistance. *Journal of Hydraulic Engineering*, HY 4(91), 1-25.

Schlichting, H. (1979). *Boundary-layer theory* (7th ed.). New York, USA: McGraw-Hill.

Sotelo, A. G. (2002). *Hidráulica de canales*. México, DF, México: Facultad de Ingeniería, Universidad Nacional Autónoma de México.